COMOTI
ROMANIAN RESEARCH & DEVELOPMENT INSTITUTE FOR GAS TURBINES

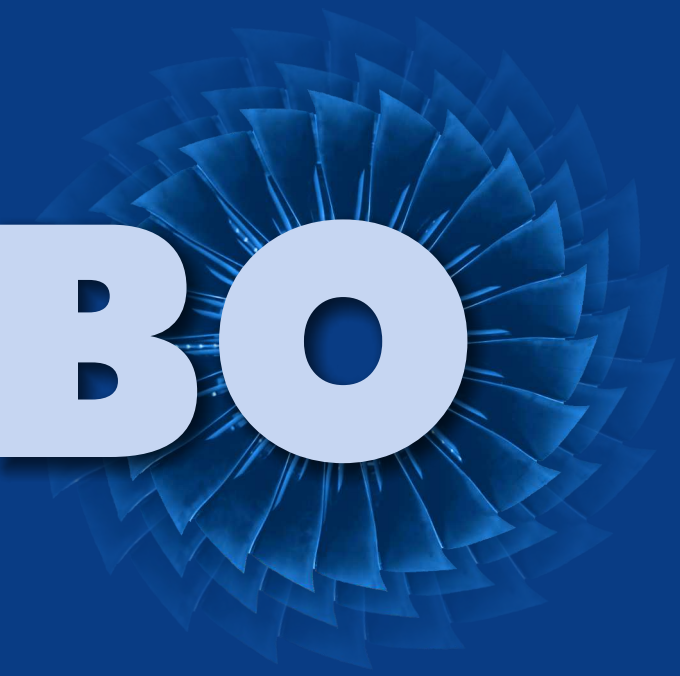

TURBO

Scientific Journal

vol. IX (2022), no. 1

SPACE AND SECURITY FOR EASTERN EUROPE

Romania - 10 years in the European Space Agency

Conference and Exhibition

May 16 - 19, 2022
Palace of Parliament, Bucharest, Romania

Organised by the Romanian Space Agency (ROSA), the event brings together the most important actors in research, academia and space industry in Romania, as well as representatives at European level, such as the European Commission and the European Space Agency (ESA).

10 years of COMOTI's presence in the European Space Agency programs

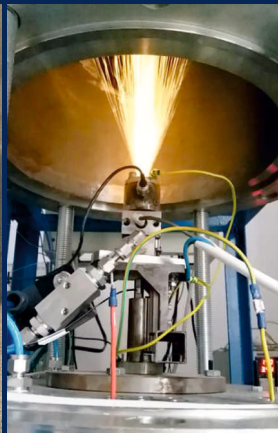

Editorial Board

More information:
http://www.comoti.ro/ro/jurnalul_stiintific_turbo.htm
jeni.vilag@comoti.ro

ISSN: 2559-608X
ISSN-L: 1454-2897

Scientific Journal TURBO is included in:
-ICI World of Journals:
ICV 2020: 60,04
https://journals.indexcopernicus.com/search/details?id=48512

-Directory of Open Access Scholarly Resources (ROAD)
https://portal.issn.org/resource/ISSN/2559-608X#

-Directory of Research Journals Indexing (DRJI):
http://olddrji.lbp.world/JournalProfile.aspx?jid=2559-608X

CONTENT

Editorial

Omul și uimirea sa

Înţepenirea nu-i o cale, nici aduce mântuire.
Înfiorarea[1] e a omului supremă calitate.
Oricât de rar ar fi, cutremurat
El simte-adânc cele măreţ-înfricoşate!

Goethe, Faust, traducere Lucian Blaga

[1]Înfiorarea, uimirea în faţa tainelor lumii şi a tiparelor ei, era, după Goethe, suprema trăire la care poate ajunge omul

Pentru a exprima realitatea din afara și dinlăuntrul său, omul a recurs la semne și combinații de semne, pentru a comunica altora ce a aflat, ce simte și ce gândește. Dintre toate sistemele de semne, cele mai utilizate sunt cele iconice și iconografice, întrucât se bazează pe asemănare, iar recognoscibilitatea este suportul redundant ce face posibilă comunicarea interumană. Asemănarea este garanția credibilității semnului cu care receptorul vine în contact nemijlocit. De aceea este în firea lucrurilor ca, atunci când percepem ceva, să ne amintească, poate bazat pe simpatie sau pe emoție, de altceva care zăcea în memoria noastră pasivă și să se adauge la ea. Este de fapt, o formă de cunoaștere prin analogie, care a fost de mare interes pentru antici și medievali. Asemănarea însă, poate induce în eroare dacă nu sesizăm deosebirile, eroare ce rezidă în echivalarea ei cu identitatea, căci asemănarea reprezintă doar un semn de identificare a celor asemănătoare și reprezintă o caracteristică structurală și/sau formală comună, a două sau mai multe lucruri, a cărei observare repetată suscită o gândire analogică.

Analogia este un cuvânt de relație, căci unicatul se raportează în primul rând la sine, fiind unicat fără comparație. Analogia ca o condiție a recunoașterii unui lucru, a permis să se poată indica și semnifica obiecte îndepărtate sau absente. Dacă lumea ar fi constituită din unicate compacte, fără asemănare între ele, ar fi o republică a originalității. Pentru că asemănarea este un liant între entități și reprezintă punte de trecere de la originalitate la banalitate, se bazează tocmai pe repetabilitate și naște adesea mirare. Mirarea însoțită de curiozitate este o însușire universală a omului, care se exercită încă din primii ani ai existenței, când descoperă treptat lumea și apoi eul, ca reacție de uimire la diversitatea lucrurilor lumii naturale anorganice, organice și vii, la cele socio-culturale și la armonia lumii.

Extraordinarul care ne zdruncină conștiința, are două origini: unele fenomene extraordinare vin din sfera timpului și spațiului familiare nouă, iar altele din însuși miezul mediului ambiental al omului ca diferențe, atitudini și degradări ale acestora. Mirarea este locul din care se naște ceva nou, o latură a lumii se relevă astfel, pentru a se lega cu dialogul, curiozitatea și riscul de a ne pune în fața necunoscutului pentru a-l îmblânzi, sau pentru a-l ocoli. Mirarea admirativă în fața unei performanțe omenești și uluirea înălțătoare își au rădăcina în conștiința faptului că este o realizare a unui semen.

Socrate a ridicat mirarea la rang de mamă a înțelepciunii. Indiferent de circumstanțele cu care-l împovărează istoria, omul nu va osteni să se mire și să se indigneze. Se miră de propria sa existență și se indignează fără putere în fața furiei cu care este distrusă planeta habitatului său. Aici începe drumul către noi orizonturi de cunoaștere. Fără uimire pe om îl așteaptă doar banalitatea repetitivității. Știința și cunoașterea nu au nici menirea și nici puterea să risipească misterul, ci doar să dezvăluie ceea ce era până atunci învăluit pentru om. Eforturile omului de a crea și de a se cunoaște pe sine, au ca finalitate indicarea limitelor lui în lume, căci extinderea și adâncirea investigațiilor asupra lumii și a omului, ne fac să devenim conștienți de puținul cunoștințelor noastre și de limitele naturii umane.

Principiul inerției, al cărui autor recunoscut este Galileo Galilei a fost descoperit intuitiv, înaintea acestuia, de Leonardo da Vinci. Însă, cum originalitatea este o chestiune de dozaj, iar unicitatea absolută nu poate fi atribuită vreunui obiect zămislit de om, gradul de originalitate ne poate arăta până unde ni se întinde umbra, momentele omului fiind, la rigoare, combinări și recombinări în fluxul valorilor.

Ec. Elena Banea,
Iulie 2021

Editorial

Man and his awe

I do not seek salvation in mere apathy
awe is the greatest boon we humans are allotted,
and though our world would have us stifle feeling,
if we are stirred profoundly, we sense the Infinite.[1]

Faust by Goethe in *Goethe's Collected Works*, Vol. 2, Edited and translated by Stuart Atkins, Princeton University Press, Chicago, 2014.

[1]*Thrill and awe in front of the world mysteries and patterns were, according to Goethe, the supreme feelings that man can experience.*

To express his outer as well as his inner reality, man chose signs and combinations of signs to be able to talk to others about his discoveries, feelings and thoughts. The most commonly used systems of signs are iconic and the iconographic systems because they rely on resemblance, and recognition, after all, is the redundant support that makes human communication possible. Resemblance is the guarantee of the credibility of the sign that the receiver comes into direct contact . Therefore, it is in the nature of things that, at the moment we perceive something, that very thing should immediately remind us, through sympathy or thrill, of something else, already existent in our passive memory and add to it. This is, in fact, a form of cognition through analogy, which was of great interest in the ancient and the medieval times. However, resemblance may be deceitful unless we seize differences, an error that resides in its reduction to identity, as resemblance represents just a sign of identification of similarities and it is a common structural and/or formal characteristic of two or several things of whose repeated observation asks for analogical thinking.

Analogy is a relating word, as oneness does primarily relate to itself, being a unique thing without any comparison. Analogy, as a condition for the recognition of a thing, has made it possible the indication and attribution of significance to far away or absent objects. If the world were made up of compact unique things, with no resemblance between them, it would be a republic of originality. Since resemblance is a link between entities, and it represents passing points from originality to commonplace, it relies on repetition and it often generates awe. Astonishment backed by curiosity is a universal characteristic of man, which is manifested from an early age of an individual while s/he gradually discovers the world around and later on her/his own ego out of wonder at perceiving the diversity of the natural nonorganic and organic worldly things, the socio-cultural environment and the harmony of the world itself.

The miracle that shatters our consciousness is twofold: some extraordinary phenomena come out of the sphere of the time and space familiar to us, while others result from the very core of man's surrounding environment as differences, attitudes and distortion of the former. Wonder is the circumstance out of which something new arises, another perspective of the world is made distinct, only to be combined with dialog, curiosity and the challenge of facing the unknown to tame or avoid it. Both awe in front of a human performance and elevating astonishment have their roots in the awareness of the fact that such performance is the achievement of a fellow human being.

Socrates raised wonder to the level of mother wisdom. Regardless of the circumstances that history loads man with, s/he shall not cease wondering and getting indignant. Each individual wonders about her/his own existence and gets hopelessly indignant against the ferocious destruction of her/his habitual planet. It is here where the path to new horizons of knowledge starts. Without wonder, all that man is left with is the common place of repetitiveness. Science and knowledge have neither the purpose nor the power to remove mystery, but to reveal what it has been previously unknown to man. However, her/his efforts to create and discover herself/himself do eventually reflect man's limits in the world since the extension and deepening of the investigations of the human nature and of the world at large make us conscious of both our limited knowledge and of the limits of the human nature as such.

The principle of inertia, whose recognized author is Galileo Galilei, has been previously discovered by simple intuition by Leonardo da Vinci. But, since originality is a matter of calibration, and absolute oneness cannot be attributed to any of man's made things, the level of originality may indicate us just how far our shadow unfolds, man's momenta rigorously being combinations and re-combinations in the flow of values.

Ec. Elena Banea,
July 2022

OIL INJECTION SCREW COMPRESSOR INITIALIZATION FILE DEFINITION FOR A 3D CFD SIMULATION

Ion MĂLĂEL[1], Valentin PETRESCU[1], Ştefan Alexandru ŞERBAN[1], Mihnea GALL[1]

Received: 02.06.2022
Accepted: 29.06.2022
Published: 06.07.2022

ABSTRACT: The positive displacement machines are used in various industry fields, having the main advantage of operating with a high-pressure ratio. But this feature causes difficulties in the efficiency evaluation with modern techniques like Computational Fluid Dynamics. In this paper, a CFD analysis without using oil injection was performed to determine the pressure distribution through the computational domain which can be used in the initialization process of the oil injection screw compressor performances simulation study. The initialization file was done without using oil injection because the CFD solver can reach more easily, without any solver crashes, to a converged solution with a periodic behaviour of the flow mainly because the flow isn't multiphase. Using this results file for initialization, the solver shall be more stable, avoiding crashes. The outlet pressure was set up to 5 bar with 1 bar on the suction side. As result, the pressure and temperature contours on the rotors and cross-plane are presented in this paper. The inlet and outlet mass flow rate evolution was evaluated too. After data post-processing, the conclusion is that the results file can be used in the initialization process for the future CFD screw compressor with oil injection simulations.

KEYWORDS: Computational fluid dynamics, screw compressor, Ansys CFX, flow initialization

1. INTRODUCTION

The nowadays energy crisis is caused by both the growing energy needs for technological evolution [1] and the outdated methods of exploiting the Earth's resources [2]. Thus, the development of new high-performance and sustainable methods [3] for resource exploitation must be on the agenda of researchers around the world.

The role of volumetric machines with positive displacement in the technological process of extraction/ processing of classical, non-renewable resources such as coal and oil is well known [4]. The screw compressor is composed of two rotors (male and female or driver and driven) whose design represents a real challenge for engineers in the field due to the shape of the rotor lobes [5].

A reference work in this field belongs to N. Stosic [6] where the algorithms that were the basis for generating a profile configuration with 3 lobes for the male rotor and 5 lobes for the female rotor are described. CFD methods can be used to evaluate the performance of a screw compressor [7]. Defining the computational domain involves the use of dedicated software [8-9] for generating the computational grid, capable of meshing volumes/ surfaces of the order of microns. In Fig. 1 the 3D CAD features for a screw compressor with oil injection are presented.

Several techniques of computational grid generation for the rotor domain of a positive displacement machine have been verified by S. Rane [10]. Their accuracy was evaluated by means of a compression process analysis inside a positive displacement volumetric machine such as a screw compressor.

Internationally, only a few studies based on the use of CFD methods are available to determine the performance of screw compressors. The commonly employed software packages are Ansys CFX [11], Ansys Fluent [12], StarCCM+ [13] and ConvergeCFD [14]. In Romania, the research of the screw compressor efficiency with high discharge pressures (that implies the presence of oil injection to ensure the sealing, reduce discharge temperature and noise) with CFD methods is at the beginning [15-16].

[1] Romanian Research and Development Institute for Gas Turbines COMOTI

The encountered problems refer to the solver stability for the multiphase analysis of volumetric machines that can power facilities [17] with high discharge pressures (i.e. exceeding 40 bar). This paper presents the definition of the initialization file that can be subsequently used in the start process of the 3D CFD simulation of a screw compressor with oil injection.

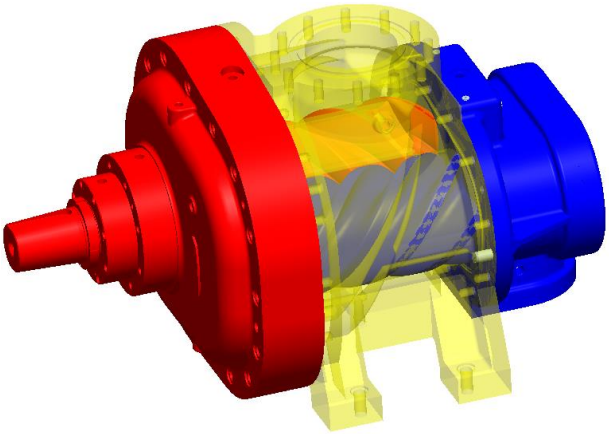

Fig. 1 3D CAD screw compressor geometry [18]

2. CFD SETUPS

The definition process of the initialization file for a 3D CFD simulation of an oil injection screw compressor done in Ansys CFX starts with the computational domain CAD modelling. Using CAD software like SolidWorks, the screw compressor geometry CAD file was imported in order to trace the working fluids paths. The computational domain was split into four subdomains to emphasize the rotating parts and the stator ones. In this way, the domain has three stator subdomains which include the suction side, pressure side, and the oil injection pipe and a rotating subdomain composed of male rotor domain and female rotor domain.

Fig.2 shows an exploded view of the computational domain done after using the boolean functions, such as unite, subtract and intersect.

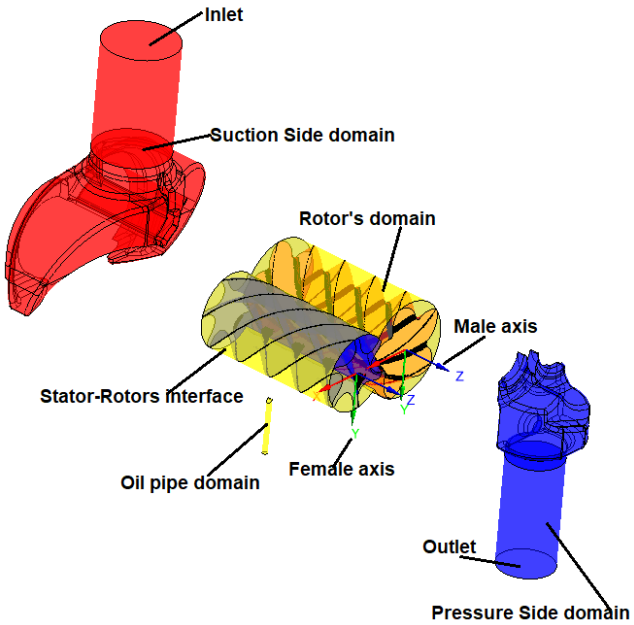

Fig. 2 Computational domain

Regarding the mesh generation for the rotors domains, the TwinMesh software was used. Thus, the shape of the lobes was imported using the curves described in a '.igs' type file. Once the geometry was imported, the main components were set up: male rotor casing, female rotor casing, male rotor and female rotor (Fig. 3). The next step was to define the interface between the male rotor and the female rotor, which was the final step in defining the geometry in TwinMesh.

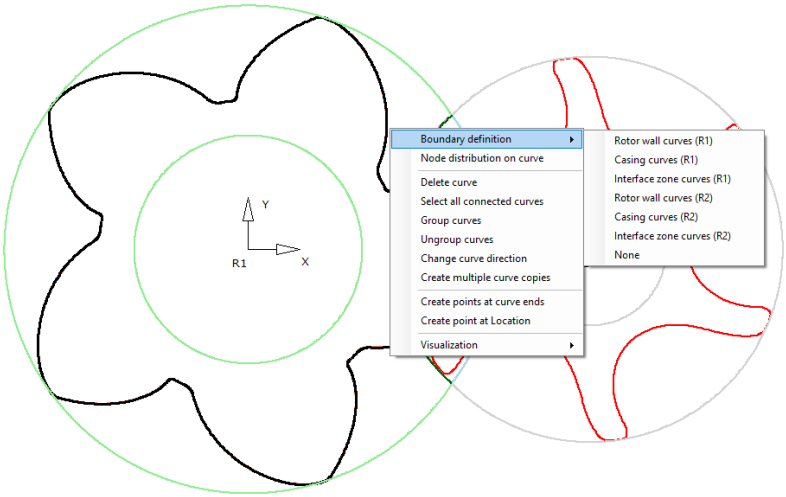

Fig. 3 Rotors geometry definition in TwinMesh[19]

Then the 2D grid parameters were set. These parameters include the type of meshing, maximum element size, first element height (inner), first element height (outer), number of elements in the radial direction, and number of elements in the z-direction. After mesh generation, a quality check was performed. The minimum angle, the aspect ratio, the volume change and determinants are assessed. Fig. 4 shows the 2D grid, while Fig.5 presents the minimum angle distribution as part of the quality check analysis.

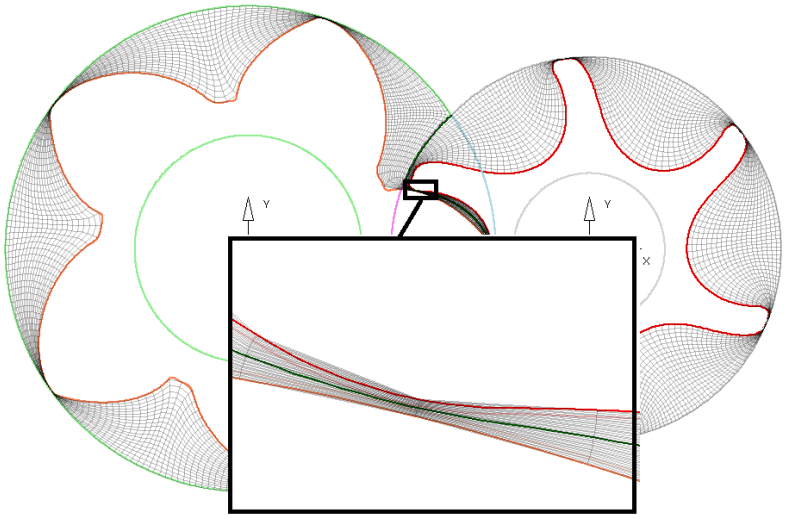

Fig. 4 Rotating 2D mesh

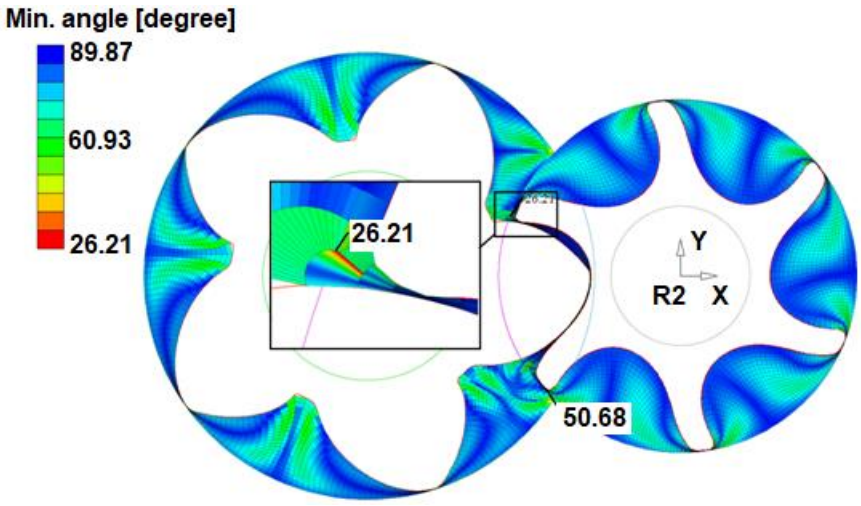

Fig. 5 Rotor's mesh quality

Starting from the stator domain CAD model that consists of three subdomains, namely: the suction area, the discharge area and the oil injection pipe (see Fig. 2) and using the Ansys Meshing software, the mesh was generated. The method used to generate the grid was MultiZone, to allow the transition from Hexaedra to Tetrahedra type elements in order to control the number of elements. To avoid problems that may occur in the interface areas between the rotor and the stator domains, the Face Sizing function was used too (see Fig. 6).

Fig. 6 shows the mesh for the entire stator domain together with the information related to the number of nodes, the number of elements and also their quality. At the same time, the area in which the above-mentioned function (i.e. face sizing) was used can be observed.

Regarding the turbulence model, the Shear Stress Transport model was used [20] and the boundary conditions (see Fig. 7 and Table 1) were set to have Opening for the screw compressor's inlet and outlet. Wall-type boundary condition was set for the oil inlet patch.

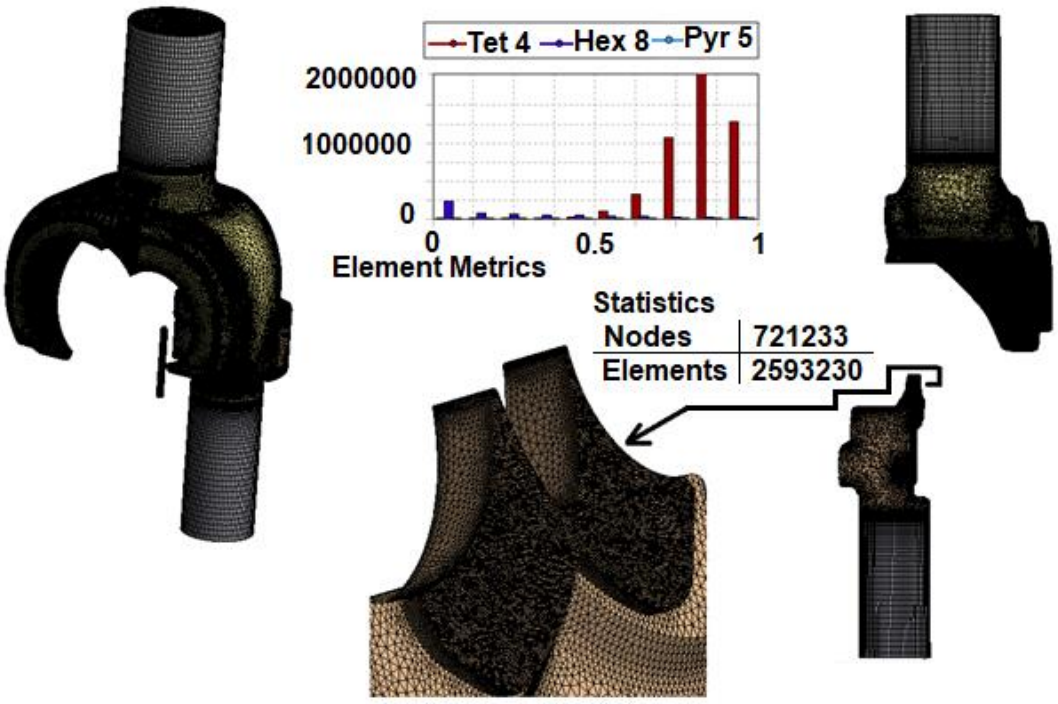

Fig. 6 Stator subdomains mesh

Table 1. Ansys CFX boundary conditions values

No.	Parameter	Value	Unit
1.	Inlet_Pressure	1	[bar]
2.	Outlet_Pressure	5	[bar]

No.	Parameter		Value	Unit
3.	Rotational speed	male	3343	[rpm]
		female	2785	[rpm]
4.	Inlet_Temperature		26	[°C]

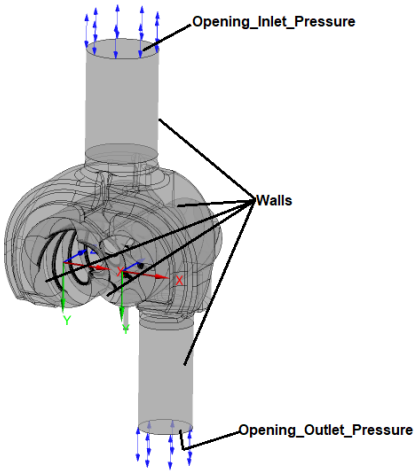

Fig. 7 Boundary conditions

3. RESULTS and DISCUSSIONS

During the initialization file numerical computation, the evolution of the working fluid pressure from the inlet to the outlet of the screw compressor was followed. In Fig.8 the distribution of the absolute pressure in a cross-plane can be observed where 'blue' represents the inlet pressure, 1 bar, and 'red' is the discharge pressure, 5bar.

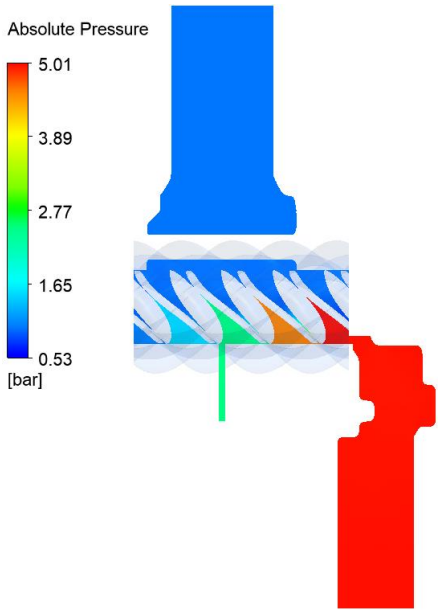

Fig. 8 Absolute pressure in cross-plane view

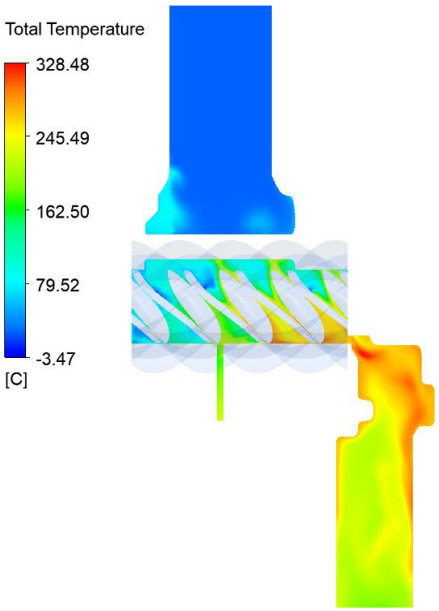

Fig. 9 Total temperature in cross-plane view

For a better understanding of the compression process, the pressure in the five volumes formed during the operation of the compressor was analyzed (Fig. 10). The first volume shows the suction pressure when this volume is still communicating with the suction port. The second volume represents the moment when the compression process starts, and the connection to the suction port is closed. The compression process continues in volumes three and four reaching volume five which is connected to the discharge port and the discharge is performed.

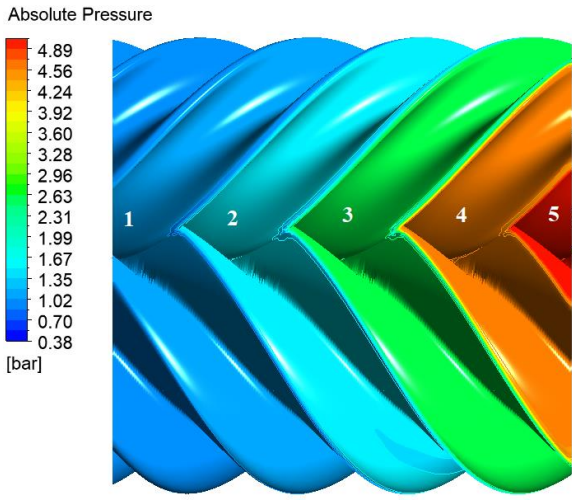

Fig. 10 Absolute pressure distribution on rotors

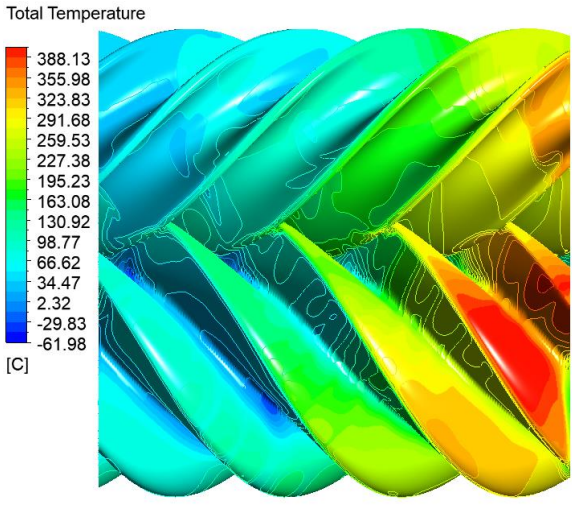

Fig. 11 Total temperature distribution on rotors

A convergence criterion of the simulation for the realization of the initialization file was represented by the periodic evolution of both the mass flow rate and the pressure. In Fig.12 the mass flow rates are presented, while Fig 13 plots the pressures.

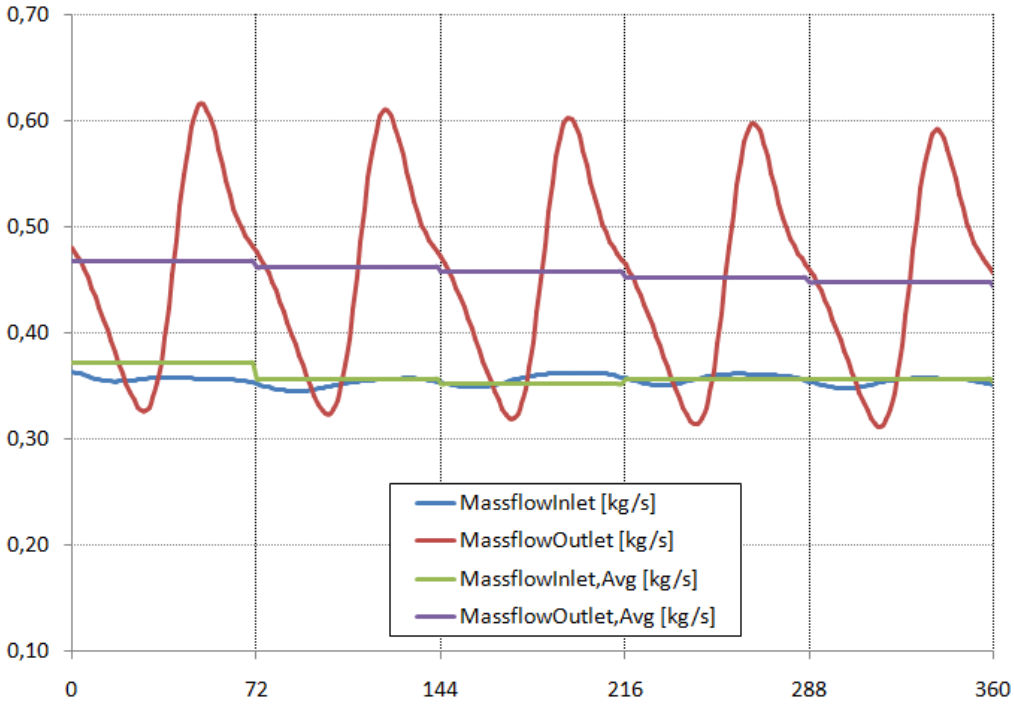

Fig. 12 Mass flow evolution over a complete revolution – 360 degrees

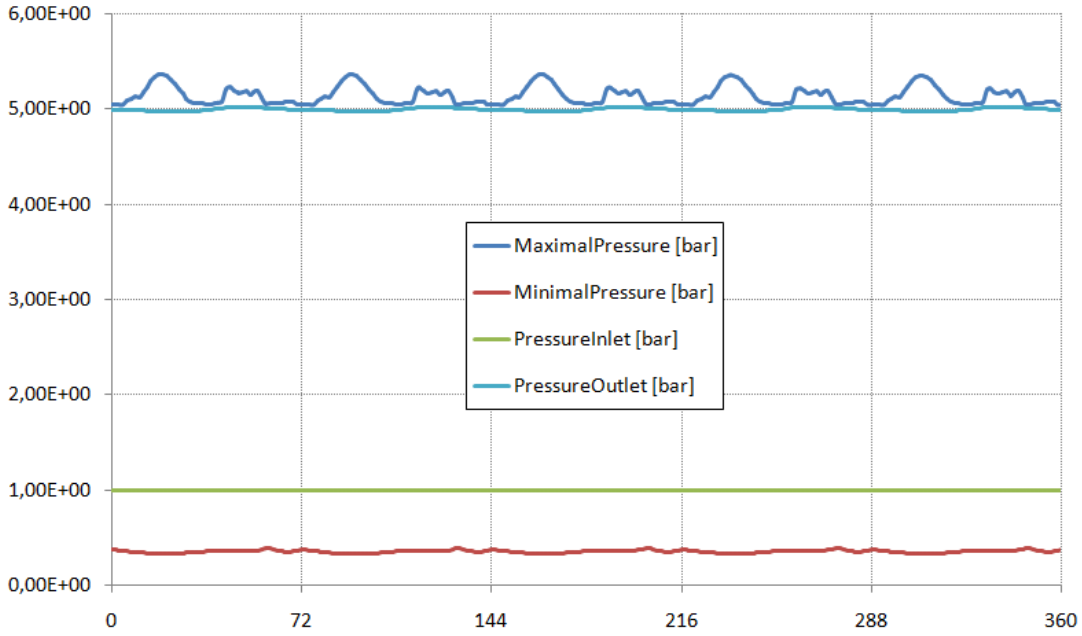

Fig. 13 Absolute pressure over a complete revolution - 360 degrees

4. CONCLUSIONS

Numerical analysis of the performance of volumetric machines with positive displacement such as screw compressors is a very important step in the pre-design phase. The stability problems of CFD solvers occur when the analysis is multiphase and the operation of the compressor takes place at high compression levels. These problems are based on the nature of the flow initiation process, which all solvers need. In this paper, the initialization file was made, which will be used in the analysis of the efficiency of an oil injection screw compressor. Thus, the aim was to obtain the periodic variation of both the inlet mass flow and the outlet mass flow in correlation with the pressure distribution in the five volumes formed by the rotor interlobes spacing and casings. For future analysis, the resulting file will be used to initialize the two-phase flow through the screw compressor.

ACKNOWLEDGEMENT

This work was supported by the Romanian Research & Development Institute for Gas Turbines COMOTI.

REFERENCES

[1]. Farmer, J. D., & Trancik, J. (2007). Dynamics of technological development in the energy sector. *London Accord Final Publication*, 1-24.
[2]. Heal, G. M. (2019). Economics and resources. In *Economics of environmental and natural resources policy* (pp. 62-73). Routledge.
[3]. Suárez-Eiroa, B., Fernández, E., Méndez-Martínez, G., & Soto-Oñate, D. (2019). Operational principles of circular economy for sustainable development: Linking theory and practice. *Journal of cleaner production*, *214*, 952-961.
[4]. Zanin, A. V., Shcherba, V. Y., Nosov, E. Y., Paramonov, A. M., Blinov, V. N., & Khrapsky, S. P. (2020). Development and Research of an Experimental Prototype of the Positive Displacement Two-Stage Piston Hybrid Energy-Generating Machine. In *Journal of Physics: Conference Series* (Vol. 1441, No. 1, p. 012129). IOP Publishing.
[5]. Shen, Z. (2020). Profile Design Method of Twin-Screw Compressor Rotors Based on the Pixel Solution. *Mathematical Problems in Engineering*, *2020*.
[6]. Stosic, N., Smith, I. K., & Kovacevic, A. (2003). Optimisation of screw compressors. *Applied Thermal Engineering*, *23*(10), 1177-1195.
[7]. Liu, G., Zhao, X., Liansheng, L., Bin, T., Qichao, Y., & Yuanyang, Z. (2019, August). Analysis on Performance of Screw Compressor in MVR system. In *IOP Conference Series: Materials Science and Engineering* (Vol. 604, No. 1, p. 012002). IOP Publishing.
[8]. Spille-Kohoff, A., Hesse, J., Andres, R., & Hetze, F. (2017, August). CFD simulation of a dry scroll vacuum pump with clearances, solid heating and thermal deformation. In *IOP Conference Series: Materials Science and Engineering* (Vol. 232, No. 1, p. 012052). IOP Publishing.
[9]. Kovacevic, A., et all. (2005, January). Design Integration for Screw Compressors. In *ASME International Mechanical Engineering Congress and Exposition* (Vol. 42118, pp. 29-33).
[10]. Rane, S., Kovacevic, A., Stosic, N., & Kethidi, M. (2013). Grid deformation strategies for CFD analysis of screw compressors. *International Journal of Refrigeration*, *36*(7), 1883-1893.
[11]. Zhang, J. W., Wu, Y. R., Hsieh, S. H., & Huang, C. S. (2019, August). Use of CFD to Investigate Flow Characteristics and Oil Distribution Inside an Oil-injected Screw Compressor. In *IOP Conference Series: Materials Science and Engineering* (Vol. 604, No. 1, p. 012016). IOP Publishing.
[12]. Basha, N., Kovacevic, A., & Rane, S. (2019, August). User defined nodal displacement of numerical mesh for analysis of screw machines in FLUENT. In *IOP Conference Series: Materials Science and Engineering* (Vol. 604, No. 1, p. 012012). IOP Publishing.
[13]. Shen, L., et all. (2019, March). Dynamic mesh technology for the simulation study of single screw expander. In *International Conference on Computational & Experimental Engineering and Sciences* (pp. 885-889). Springer, Cham.
[14]. https://convergecfd.com/applications/compressors-fans-and-blowers
[15]. Mălăel, I., Sima, M. Numerical, investigation of a screw compressor performance, TURBO, vol IV(2017, no 2).
[16]. Ion, M., et all. (2018, August). Numerical efficiency evaluation of a high pressure ratio screw compressor. In *2018 5th International Conference on Mathematics and Computers in Sciences and Industry (MCSI)* (pp. 1-6). IEEE.
[17]. Șerban, Ș. A., Tomescu, S. G., Vlăducă, I., & voicu, S. Energy improvement of an oil injected screw compressor skid, EMERG, Volume VII, Issue 1/2021 ISSN 2668-7003, ISSN-L 2457-5011.
[18]. http://www.comoti.ro/en/Compresoare-cu-surub.htm
[19]. https://www.twinmesh.com/project/reliable-cfd-analysis-of-screw-compressors-and-expanders/
[20]. R. Menter, Two-Equation Eddy-Viscosity Turbulence Models for Engineering Applications, AIAA Journal, 32(8):1598-1605, ISSN: 0001-1452, EISSN: 1533-385X, August 19

VANED DIFFUSER NUMERICAL INVESTIGATION FOR MICROJET ENGINE

Mihnea GALL[1], Valeriu DRĂGAN[1]

Received: 23.05.2022
Accepted: 29.06.2022
Published: 06.07.2022

ABSTRACT: The current paper presents an approach for designing the vaned diffuser for a micro gas turbine engine, with high pressure ratio and small overall diameter. A particular challenge in this field is to increase the cycle pressure ratio while maintain aerodynamic performance and not exceeding the imposed engine diameter. Recently mixed flow and semi-diagonal configurations have been proposed for such applications; however, they often fall in-between the design rules of either axial or radial compressors. We attempt to rationally combine the existing know-how with full viscous CFD simulations in order to obtain an optimal design for our case-study. Both rotor and diffuser are of original design and have been optimized using full viscous CFD RANS. Since the microjet engine size is of ~40 daN thrust, it falls into the category of affordable as well as technically useful UAV-size powerplants, we hope that it will be more relevant to the field.

KEYWORDS: mixed flow diffuser, semi-diagonal diffuser, high performance compressor, diffuser databook

1. INTRODUCTION

In the last decades, significant research efforts have been oriented towards the field of micro gas turbine (MGT) and microjet engines with the final goal to find a game changing system and performance improvement. The ongoing concern on greenhouse gas emissions forces worldwide nations to adopt drastic regulations in terms of carbon emissions reduction and efficiency increase. This policy is expected to drive the MGT/microjet market in the next years, from a 26 million USD in 2021 to a 61 million USD in 2030, with a compound annual growth rate of 10% [1]. The MGT/microjet high energy density and high power density features make them very attractive for different applications, ranging from military and civil unmanned aerial vehicles (UAV), model aircraft, gliders, air taxi, cargo aerial vehicles, ultra-light aircraft, hybrid electric vehicles to portable power plant applications and auxiliary power units (APU) [2].

In a very dynamic market economy, the microjets must possess several advantages compared to other competing technologies such as batteries and fuel cells. The microjets exhibit enhanced redundancy and reliability, enhanced operational flexibility and high energy density [3]. Despite their low overall system efficiency, the power to weight ratio is still higher compared to the exiting batteries as a relatively short time is needed to extract energy from the stored fuel.

However, one has to mention some disadvantages of microjets. Namely, overall efficiency figures are low and a simple downscaling of highly efficient large gas turbine engines is not the path towards a good microjet due to significant change in Reynolds number, enhanced heat transfer between the hot and cold parts of the engine, as well as material and manufacturing challenges of miniaturized engines [4].

In general, the compression unit of microjets consists of a single centrifugal stage, either pure radial type or mixed flow type. Centrifugal compressors are shorter, cheaper and less complex compared to their axial counterparts. Moreover, centrifugal compressors have higher pressure ratio per stage, wider operating range

[1] Romanian Research and Development Institute for Gas Turbines COMOTI, Bucharest, Romania

and they are reported to resist better to foreign objects impact, thus having greater reliability and longer lifetime [5]. To reduce the frontal area of the engine, diameter constraints are usually imposed in the design of microjets compression units and so challenges appear in the design of radial diffusers (tradeoff between radial extension and diffusion). The transition from the impeller exit to the axial combustion chamber inlet may be designed either by a pure radial diffuser, a 90° bend and an axial de-swirl cascade, or by a more optimized crossover diffuser reminiscent of mixed flow compressors. As the overall engine performance and efficiency are strongly dependent on the compression system design, there is a clear need for compact high-performance compressors. Based on existing literature, a Thrust vs Diameter power law correlation (see Fig.1) is usually employed for pre-design engine diameter estimation. The points'labels identify the different manufacturers cited in the reference part (letters distinguish between different engines of the same manufacturer) [21-26].

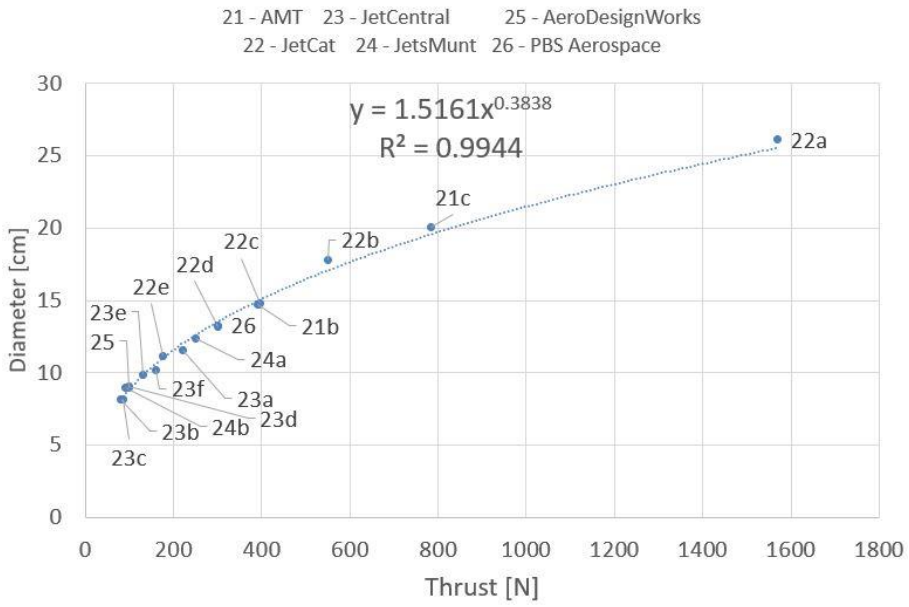

Fig. 1 Thrust vs Diameter correlation

Clear design methodologies for compact axial to radial microjet diffusers are scarce in the literature. Van der Merwe [6] and Krige [7] developed a meanline code for microjet radial vaned diffuser design based on theory of Aungier [13]. The code was used together with CFD for optimization of the 20 daN BMT-120 [9] microjet engine. Subsequently, de Villiers [8] focused on the development and optimization of conventional radial diffusers for the same BMT-120 engine using meanline codes as a starting point. A novel crossover design strategy was implemented by Burger [10] with the aim to prove the possibility of replacing the conventional radial to axial 90° bend followed by axial de-swirling vanes with a crossover diffuser. Diener [11] and Kock [12] investigated the suitability of mixed flow impellers to be integrated into microjet engines along with a crossover diffuser configuration**.**

The microjet diffuser design methodology commonly starts from a 0D/1D meanline code from Japikse [14], Aungier [13] or Cumpsty [15]. Afterwards, experimental correlations and databooks are used to define the main diffuser paramters. Then, a 3D CAD design follows along with a CFD validation. The final design according to the requirements of the specific application comes as a result of an optimization process in a quite large optimization space which is in general very time-consuming and requires significant computational effort and capabilities.

Verstraete et al. [16] performed a multidisciplinary optimization (high efficiency and low centrifugal stress) applied to a radial microjet compressor using 23 design parameters in a genetic algorithm together with an artificial neural network. By means of a similar approach, Sakaguchi et al. [17] performed a multipoint multi-objective optimization on a low solidity circular cascade diffuser using 7 design parameters. More recently, Verstraete [18] employed a bounded Kriging metamodel-assisted optimization approach for a centrifugal compressor with a final 2.59% efficiency improvement compared to the baseline design. The number of design parameters to be tuned by the optimization is 34, while the objectives ask for the maximum efficiency at two different operating points.

As the optimization usually takes place in large design spaces, parametric studies [19] by means of DOE approach (Design of Experiments) are of critical importance for the sensitivity of performance parameters with respect to the design parameters. Eventually, a common approach towards validation, that is used by both universities and research centers, is the experimental assessment by means of linear cascades facilities, as this setup is cost effective and allows rapid prototyping.

The aim of this paper is to present a possible design methodology for radial to axial compact diffusers of microjet engines. Starting from documented design input data, 4 vaned diffuser designs for a 40 daN microjet engine are generated and validated with the existing correlations and design in the literature. Eventually, the 4 designs are numerically investigated and a reference design is chosen by means of performance parameters tradeoff.

2. DESIGN APPROACH

The design input data (see Table 1) for the 4 diffuser designs (referred in the following as V1-V4) comes from previous rotor design studies. One should note that the rotor geometry is frozen and serves as an input data for the current design study. The stator pre-design starts with the outlet channel height computation using mass conservation and the static quantities computed analytically from the stator outlet total quantities imposed and the associated kinematic conditions. As a result, the outlet channel height yields 5 mm. The 75 mm stator outlet shroud radius is imposed following the R^2=0.99 power law correlation presented in Fig.1 where the input thrust is 40 daN. A maximum residual swirl of 30° is considered acceptable before entering the combustor as presented in Japikse [14].

For the vaneless diffuser part, design recommendations from the literature [13][14] are followed to avoid the stall of the component and to improve diffusion. The vaneless diffuser design parameters for the current designs are reported in

Table **2**. The vaneless diffuser stability is assessed using the plot in Fig. 2 where a critical vaneless diffuser inlet angle that divides stable from unstable regimes is defined. For the current designs, a value of $\boldsymbol{b_2/r_2}$ of approximately 0.01 along with an inlet Mach number lower than 1, translates into the inlet flow angle being smaller than 75° to accomplish stability.

Table 1 Input data & stator design constraints

Input data	
Mass flow rate	0.7 kg/s
Rotor outlet total pressure	5.39 bara
Rotor outlet static pressure	3.07 bara
Rotor outlet absolute Mach	0.92
Rotor outlet absolute velocity	375 m/s
Rotor outlet total temperature	479.3K
Rotor outlet absolute radial velocity	142.7 m/s
Rotor outlet absolute tangential velocity	346.7 m/s
Absolute velocity flow angle (wrt axial)	67.6°

Stator design constraints	
Stator outlet shroud radius	75 mm
Stator outlet target flow angle	30°
Stator outlet target velocity	130 m/s
Stator outlet target total pressure	5 bara

Table 2 Vaneless diffuser design parameters

Parameter	V1	V2	V3	V4
r_3/r_2	1.09	1.09	1.09	1.14
r_3/r_2	1.16	1.16	1.16	1.20
b_2/r_2	0.094	0.094	0.094	0.094
α_2	67.76°	68.3°	70.4°	68.5°
M_2	0.93	0.92	0.94	0.95

where $\mathbf{r_3}$- vaneless diffuser outlet radius, $\mathbf{r_2}$ –rotor outlet radius, $\mathbf{b_2}$- rotor outlet channel height, $\mathbf{M_2}$ – rotor outlet Mach number, $\boldsymbol{\alpha_2}$ – rotor outlet absolute flow angle.

As the literature prescriptions for vaned diffuser design mainly rely on statistical databooks and correlations, the starting point in the current work for vaned diffuser design is represented by the statistical approach provided by Howell and Lieblein that is mainly employed for design of axial cascades. Subsequently, the designs are plotted on typical statistical databooks coming from channel and cascade diffusers [14]. Starting from the imposed inlet and outlet flow angles of the diffuser, Lieblein provides an information about the solidity. The chord estimation uses a minimum Reynolds number of $\mathbf{4 \cdot 10^5}$ to stay in the turbulent area of the Moody diagram. Using rotor outlet static density, rotor outlet radial velocity and the dynamic viscosity corresponding to the rotor outlet static temperature, the chord can be evaluated. Using the solidity definition, a first information on the number of vanes can be determined. Starting from this pre-design approach, 4 vaned

diffusers are designed in order to assess their performance. The main parameters of the 4 different designs are summarised in Table 3. Figure 4 plots the pressure recovery coefficient Cp as a function of the aspect ratio (AS) for a given Mach number and for different values of the blockage factor B. One can understand that the maximum pressure recovery coefficient is always located in the proximity of unity aspect ratio.

In the current designs, the V4, V2 and V1 aspect ratio (computed for the splitter) is close to 1, while for V3 the aspect ratio departs from 1 where the C_p starts to decrease. In Fig.3 we plot a correlation in terms of channel length to width ratio (L/W), area ratio and C_p. The locus of the designs that are investigated in this paper is thus placed outside the unsteady regions, with the best C_p predicted for V4 design.

Table 3 Vaned diffuser design parameters

Parameter	V1	V2	V3	V4
Number of vanes	26	33	15	37
Stagger angle	52.6°	52.6°	52.6°	45.8°
Solidity (main blade)	1.85	2.35	1.07	2.22
Aspect ratio (main) AS	0.85	1.12	0.42	0.71
Aspect ratio (splitter) AS	1.371	1.84	0.69	1.16
Area ratio AR	1.98	2	2.09	2.13
Length/Width L/W	5.1	7	2.6	6

where C_p is the pressure recovery coefficient, the solidity is defined as the chord to pitch ratio, while the aspect ratio is defined as the channel height to width ratio.

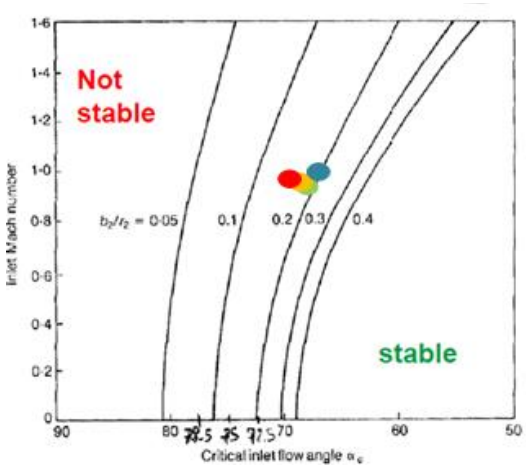

Fig. 2 Vaneless diffuser stability [20]

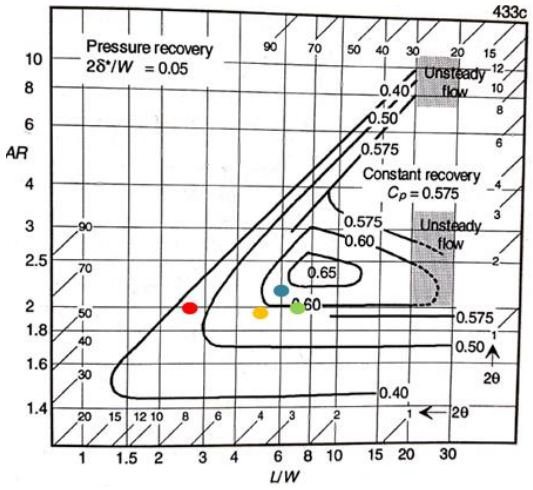

Fig. 3 Correlation of L/W, AR and Cp [14]

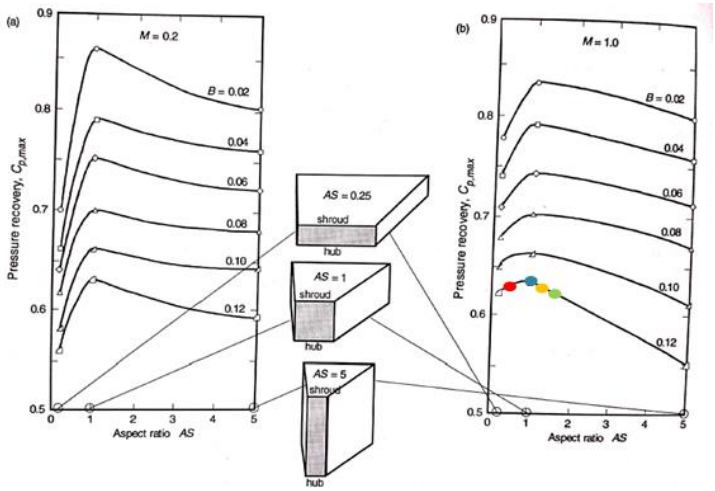

Fig. 4 Pressure recovery coefficient vs Aspect ratio [14]

3. NUMERICAL SIMULATIONS

The 3D geometry of the diffusers (hub & shroud curves, blades) is defined using Ansys BladeGen. The structured computational grid is generated using Ansys TurboGrid with the wall first cell size of 1 micron. For both the rotor and the stator, periodicity conditions are employed to reduce the computational effort. Steady state RANS simulations are performed using ANSYS CFX solver. The boundary conditions and the computational domain statistics are described in Table 4. The non-dimensional wall y+ distribution for the rotor domain and for the V4 stator domain are presented in Fig.5.

Table 4 Boundary conditions and computational domain statistics

Inlet (rotor)	Total pressure: 1 bara Total temperature: 288 K
Outlet (stator)	Mass flow rate: 0.7 kg/s
Walls	Adiabatic, no slip
Rotational speed (rotor)	80000 RPM
Turbulence model	SST k-omega

Rotor	2 397 900 cells
Stator V1	1 564 056 cells
Stator V2	1 666 008 cells
Stator V3	1 733 670 cells
Stator V4	1 034 098 cells

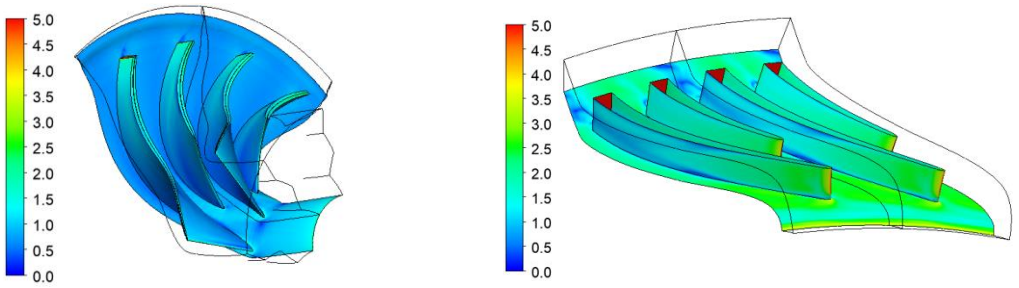

a. rotor **b. V4 diffuser**

Fig. 5 Dimensionless y+ distribution

4. RESULTS

The inlet to outlet mass averaged static pressure and the inlet to outlet mass averaged total pressure in stationary frame are plotted in Fig. 6 and Fig. 7 respectively, for the 4 investigated designs. The comparison in terms of the main performance parameters of the 4 designs is summarized in Table 5. Fig. 6 shows that V2 performs the best in terms of static pressure recovery, while V3 has the lowest static pressure recovery. This is also shown by the C_p values in Table 5 (0.62 for V2 and 0.51 for V3). The highest total to total pressure ratio is recorded for V2, followed by V1, V4 and V3 as shown in Fig. 7 too. V2 and V4 are very close in terms of total to total isentropic efficiency, however the de-swirl capability of V4 (28.7°) outperforms V2 **(**46°). V1, V2 and V3 have the same geometry for the vaneless diffuser. As the vaneless space acts as a regulating valve, it impacts on the rotor static pressure evolution and so V4 rotor static pressure trend differs from V1 (with V2 and V3 superimposed on V1).

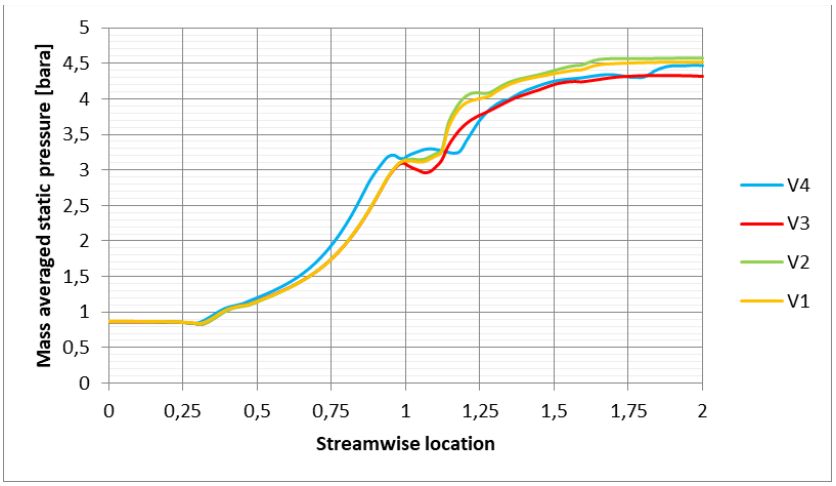

Fig. 6 Inlet to outlet mass averaged static pressure (entire stage)

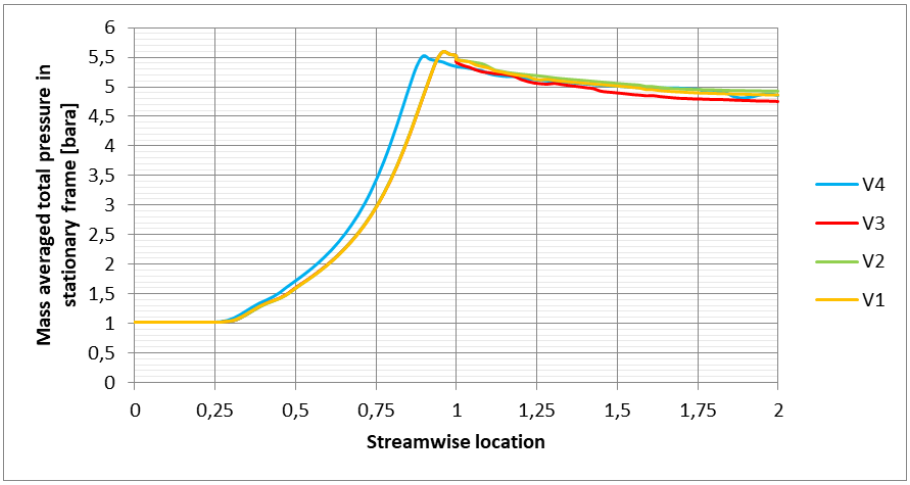

Fig. 7 Inlet to outlet mass averaged total pressure in stationary frame (entire stage)

Table 5 Main performance parameters

Parameter	V1	V2	V3	V4
Number of vanes	26	33	15	37
Total to total pressure ratio	4.8	4.86	4.68	4.78
Outlet static pressure (bara)	4.51	4.57	4.32	4.46
Outlet flow angle (from axial direction)	-47.3°	-46°	-50°	-28.7°
Outlet velocity (m/s)	134.2	130	147	134
Total to total isentropic efficiency	0.837	0.849	0.815	0.841
Pressure recovery coefficient C_p	0.59	0.62	0.51	0.59

Table 6 Relative performance parameters compared to reference design

Parameter	V1	V2	V3
Total to total pressure ratio	0.42%	1.67%	-2.09%
Outlet static pressure	1.12%	2.47%	-3.13%
Outlet flow angle (from axial direction)	-64.81%	-60.28%	-74.2%
Outlet velocity	-0.15%	2.99%	-9.7%
Total to total isentropic efficiency	-0.48%	0.95%	-3.09%
Pressure recovery coefficient C_p	0%	5.08%	-13.55%

A weighted average using C_p, total to total isentropic efficiency and outlet flow angle was used as a criterion to compare the 4 designs. While V1, V2 and V3 scored 0.84, 0.87 and 0.78 respectively, V4 scored 0.98. As a result, V4 is considered the reference design (the best design) and relative performance parameters (see

Table **6**) are computed with respect to V4. The positive values indicate better performance, while negative values show detrimental performance compared to the reference. While V3 has poor performance for all the investigated parameters, V1 and V2 suffer from the de-swirl capability. V2 shows better performance of 1.67% for the total to total pressure ratio and approximately 5% for the C_p compared to V4, however it is not able to remove the tangential flow component. A microjet cycle analysis revealed a 7.6% thrust reduction if the engine operates with V3 instead of V4. However, the cycle analysis was not able to take into account the combustion chamber inlet flow angle and velocity influence.

The velocity contours in the blade to blade view for the V4 design and the V3 design (poor performance design) are plotted in Fig. 8 and Fig. 9 for 50% and 20% of the span respectively. From Fig. 8, one can undertand that the chosen reference design is free of recirculation zones both at midspan and 20% of the span, except the wake zone in the blades trailing edge. In contrast, for V3, full channel recirculation zones can be seen in Fig. 9b. at 20% span, while the 50% span shows a splitter trailing edge flow detachment. This impacts on the blade loading and so on the diffusion process.

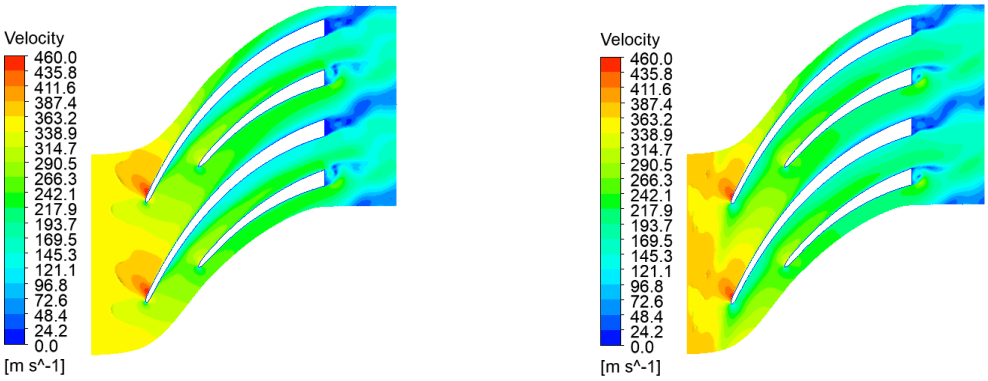

a. 50% span **b. 20% span**

Fig. 8 Velocity contour in blade to blade view – V4 design

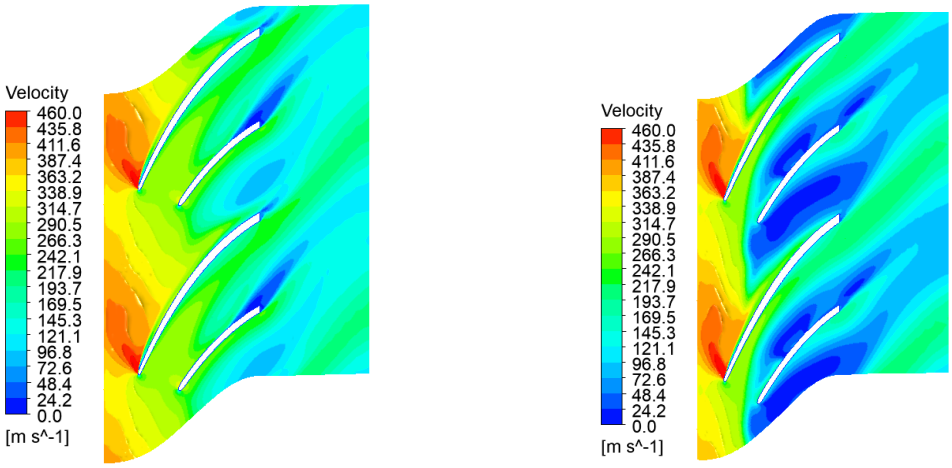

a. 50% span **b. 20% span**

Fig.9 Velocity contour in blade to blade view – V3 design

5. CONCLUSIONS AND FURTHER WORK

To conclude, 4 compact radial-to-axial microjet diffusers were designed and validated against the available correlations and databooks available in the literature. The vaneless diffuser design is verified using stability criteria, whereas the vaned diffuser design is checked using aspect ratio, area ratio and length to width correlations for the pressure recovery coefficient.

The 4 designs were numerically investigated and their performance parameters were thoroughly compared to establish the best design. A diffuser with 37 vanes was chosen to deliver the best performance for this particular 40 daN microjet application with a pressure recovery coefficient of 0.59, a total to total pressure ratio of 4.78 and an outlet flow angle of approximately 29°.

A natural step further is to perform a parametric analysis using CFD tools to understand the relative influence of different design parameters in the diffuser performance. One expects to obtain new correlations that are fully adapted to the microjet diffusers. Following this result, an optimization campaign using state-of-the-art techniques shall be applied to the baseline design to eventually define several candidates to be experimentally validated.

REFERENCES

[1] Aircraft Micro Turbine Engines Market, https://www.marketsandmarkets.com/Market-Reports/aircraft-micro-turbine-engines-market-248924999.html?gclid=Cj0KCQiArt6PBhCoARIsAMF5wajZnXK2WBYc_RfSzGQcM8xGGVRLkVFl7zRWvYYTpEq3yxxQLhltqZ0a Accessed on 12th February 2022

[2] Marcellan, A. (2015), An exploration into the potential of microturbine based propulsion systems for civil Unmanned Aerial Vehicles, MSc Thesis, TU Delft, Thesis number = 030#15#MT#FPP

[3] Decuypere, I.R., & Verstraete, D. (2005). Micro Turbines from the Standpoint of Potential Users, Micro Gas Turbines - Educational Notes RTO-EN-AVT-131, Paper 15, pp. 15-1-15-14.
[4] Van den Braembussche, R.A., (2205) Micro Gas Turbines - A Short Survey of Design Problems, Micro Gas Turbines - Educational Notes RTO-EN-AVT-131, Paper 1, pp. 1-1 -1-18
[5] Dodge et al. (1987), High efficiency transonic mixed-flow compressor method and apparatus, United States Patent, Patent Number 4678398
[6] van der Merwe B.B. (2012), Design of a Centrifugal Compressor Impeller for Micro Gas Turbine Application, MSc Thesis, Stellenbosch University, ISSN-L 2310-7855 http://hdl.handle.net/10019.1/71610
[7] Krige D.S. (2013), Performance Evaluation of a Micro Gas Turbine Centrifugal Compressor Diffuser, MSc Thesis, Stellenbosch University, ISSN-L 2310-7855, http://hdl.handle.net/10019.1/80119
[8] de Villiers L.C.B. (2014), Design of a Centrifugal Compressor for Application in Micro Gas Turbines, MSc Thesis, Stellenbosch University, ISSN-L 2310-7855, http://hdl.handle.net/10019.1/96052
[9] Oppong, F, van der Spuy SJ, von Backström T. W. (2017), Upgrading the BMT 120 KS Micro Gas Turbine., R & D Journal of the South African Institution of Mechanical Engineering 2017, 33, 22-31.
[10] Burger C.J. (2016), Design Procedure of a Compact Aerodynamic Crossover Diffuser for Micro Gas Turbine Application, MSc Thesis, ISSN-L 2310-7855, http://hdl.handle.net/10019.1/98634
[11] Kock M.P. (2017), Design of a Cross-over Diffuser for a Mixed Flow Compressor Impeller, MSc Thesis, Stellenbosch University, ISSN-L 2310-7855, http://hdl.handle.net/10019.1/100997
[12] Diener, O.H.F et al. (2016), Multi-Disciplinary Optimization of a Mixed-Flow Compressor Impeller, Turbo Expo: Power for Land, Sea, and Air, vol. 8. ASME
[13] Aungier, R.H. (2000), Centrifugal compressors: a strategy for aerodynamic design and analysis, American Society of Mechanical Engineers, 2000, ISBN 0-7918-0093-8
[14] D. Japikse (1996),Centrifugal Compressor Design and Performance,Concepts ETI, ISBN 0-933283-03-2
[15] N.A. Cumpsty (1989) , Compressor aerodynamics, Longman Scientific and Technical, ISBN 0-582- 01364-X
[16] Verstraete, T., Alsalihi, Z., and Van den Braembussche, R. A. (March 24, 2010). Multidisciplinary Optimization of a Radial Compressor for Microgas Turbine Applications, ASME. J. Turbomach. July 2010; 132(3): 031004. https://doi.org/10.1115/1.3144162
[17] Sakaguchi, D, Ishida, M, Hayami, H, Mueller, L, Alsalihi, Z, & Verstraete, T. (2014), Multipoint Multi-Objective Optimization of a Low Solidity Circular Cascade Diffuser in Centrifugal Blowers, Proceedings of the ASME Turbo Expo 2014: Turbine Technical Conference and Exposition. Volume 1A: Aircraft Engine; Fans and Blowers. Düsseldorf, Germany. June 16–20, 2014. V01AT10A018. ASME. https://doi.org/10.1115/GT2014-26013
[18] Aissa, Mohamed H., and Tom Verstraete, 2019, "Metamodel-Assisted Multidisciplinary Design Optimization of a Radial Compressor" International Journal of Turbomachinery, Propulsion and Power 4, no. 4: 35. https://doi.org/10.3390/ijtpp4040035
[19] Zhou, L., Wang, Z.X., & Liu, Z.W. (2014), Investigation on influence of design parameters for tandem cascades diffuser using doe method, Engineering Applications of Computational Fluid Mechanics, 8(2), 240-251.
[20] Gaetani P. (2020), Turbomachinery course lecture notes, Politecnico di Milano, ID097354
[21] AMT: http://www.amtjets.com/specs.php accessed on 13th February 2022 (a-Titan, b-Nike, c-Lynx)
[22] JetCat: http://www.jetcatamericas.com/ accessed on 13th February 2022 (a-P550Pro, b-P400Pro, c-P300Pro, d-P180NX, e-P220RX)
[23] JetCentral: https://www.jetcentral.com.mx/products/turbines/ accessed on 13th February 2022 (a-Bee80, b-Hornet85, c-Rabbit100, d-Lynx130, e-Cheetah160, f-Mammoth250)
[24] Jets-Munt: https://jets-munt.com/ accessed on 13th February 2022 (a-VT90BLR, b-M100XBL)
[25] Aerodesign Works B300F: https://www.aerodesignworks.com/en/products/model-jet-turbines/
[26] PBS Aerospace TJ40-G2: https://www.pbsaerospace.com/turbines

DESIGN AND ANALYSIS OF SUPERSONIC TURBINE ROTOR BLADES

Alexandru HANK[1], Cosmin Petru SUCIU [1], Daniel USERIU[1], Gabriel BADEA[1], Teodor STANESCU[1], Mihai Cornel TĂRĂBÎC[1]

Received: 31.05.2022
Accepted: 30.06.2022
Published: 06.07.2022

ABSTRACT: In this paper, the supersonic vortex flow design method was used in order to achieve the two-dimensional blade profile geometry for a supersonic turbine rotor operating at conditions similar to an existing pneumatic turbine starter used for gas turbines of 4MW power output. Based on the vortex flow theory, a MATLAB code was developed which require basic inputs that are generally known for a turbine rotor design. A CFD simulation has been done using ANSYS FLUENT solver in order to validate the analytical calculations. The velocity field has been properly developed between the blades. The location of the complex wave system generation, as well as the intersection point between the expansion and compression waves has been compared to the analytical computation and the results shown an acceptable error.

KEYWORDS: Supersonic, Turbine, Vortex flow, Rotor, Method of Characteristics, CFD

NOMENCLATURE

Symbols:

- $\boldsymbol{V}$ - Velocity
- $\boldsymbol{R}$ - Radius
- $\boldsymbol{R^*}$ - Dimensionless radius
- $\boldsymbol{M}$ - Mach number
- $\boldsymbol{\nu}$ - Prandtl-Meyer angle
- $\boldsymbol{\gamma}$ - Specific heat ratio
- $\boldsymbol{\alpha}$ - Circular arcs turning angle
- $\boldsymbol{\beta}$ - Flow angle
- $\boldsymbol{\varphi}$ - Major vortex-expansion-characteristic function
- $\boldsymbol{G^*}$ - Dimensionless blade spacing
- $\boldsymbol{C^*}$ - Dimensionless chord
- $\boldsymbol{x^*}$ - Dimensionless x coordinates
- $\boldsymbol{y^*}$ - Dimensionless y coordinates
- $\boldsymbol{m}$ - Slope

Subscripts:

- $\boldsymbol{l}$ - Lower
- $\boldsymbol{u}$ - Upper
- $\mathbf{i}$ - Inlet
- $\boldsymbol{o}$ - Outlet

[1] Romanian Research and Development Institute for Gas Turbines COMOTI

1. INTRODUCTION

Many energy-recovery cycles, drive cycles (Organic and Steam Rankine cycles) and rocket propulsion cycles require the use of a turbine that operates at low volumetric flow and high-pressure ratio. Additional requirements include low cost, reduced weight, and reduced axial length.

These types of applications are usually best fitted with a special class of turbomachinery referred to as supersonic turbines or highly-loaded turbines. This type of mechanical system is usually described by constant pressure, or small pressure variations at the inlet and outlet of the turbine rotor. Supersonic turbines gained interest from the industry in the 1950s when lighter turbines meant lower manufacture and operational costs. Verneau et al analysed turbines for solar plants and waste energy recovery systems [1]. The university of Hannover has tested and ORC supersonic turbine generator with partial admission that successfully operated in a power range of 2-8 kW.

Noraiz M. et al [5] have studied supersonic turbine blades designed with Method of Characteristics coupled with a RDE (rotating detonation engine). Their analyses revealed that this type of assemblies can achieve efficiencies of up to 70%. Chao Fu et al. [6] have done unsteady CFD numerical analysis to evaluate the coupling between the stator and the rotor. Their study found that high circumferential velocity at the vane outlet and short blade lead to high radial pressure gradient, which makes the low kinetic energy moves towards hub region and produce additional loss. Shin Bong-Gun [7] has studied the effect of inlet voundary condition on flow characteristics of a supersonic turbine. They have compared a pressure far field inlet condition to simulate the inlet in a supersonic rotor. The study shows that a CD nozzle will predict more accurately the supersonic flow within a turbine cascade than pressure far field boundary does.

To maximize the specific power, the degree of reaction is traditionally very low [3]. The design of such impulse turbine type rotors can be achieved using the method of characteristics to create a vortex flow inside the rotor. For enabling shockless supersonic flow between two circular arcs, a vortex flow is necessary instead of a uniform parallel flow which is usually obtained from the guide vanes.

1.1 Supersonic Vortex Flow Theory

The need of vortex type of flow is obvious when it is realized that the maximum loading for a given peak surface pressure is obtained by uniform upper and lower surface pressures created through the use of vortex flow. Supersonic vortex flow is an irrotational flow where the streamlines within are concentric circles with constant velocity along any particular streamline [4].

$$VR = Constant \tag{1}$$

Equation (1) [4] can be rewritten in terms of non-dimensional values as follows:

$$M^*R^* = 1 \tag{2}$$

where:

V – velocity R – Radius

R* - non-dimensional radius (R/r*) M* - non-dimensional velocity ratio (V/a*)

The blades designed through supersonic vortex flow theory consist of three major parts: inlet transition arcs; circular arcs; outlet transition arcs. The inlet transition arcs are required to convert the assumed uniform parallel flow at the blade inlet intro vortex flow. The concentric circular arcs turn and maintain the vortex flow. The outlet transition arcs reconvert the vortex flow into uniform parallel flow at the blade exit. The flow properties in steady supersonic flow cand be identified through the Method of Characteristics (MoC). Characteristic lines divide the flow field into a finite number of regions where flow properties are assumed to be constant. The inlet Mach number is reduced to the pressure side level and increased towards the suction side level through the transition arcs. The transition arcs are made of a sequence of straight-line segments that change with the flow direction, intersecting the straight Mach lines.

Considering isentropic flow turning at supersonic speeds, the required flow deviation to achieve a targeted Mach number can be computed using Prandtl-Mayer angle, defined in Equation (3)[4].

$$\nu = \frac{\pi}{4}\left(\sqrt{\frac{\gamma+1}{\gamma-1}} - 1\right) + \frac{1}{2}\left\{\sqrt{\frac{\gamma+1}{\gamma-1}}\, sin^{-1}[(\gamma-1)M^{*2} - \gamma] + sin^{-1}\left(\frac{\gamma+1}{M^{*2}} - \gamma\right)\right\} \tag{3}$$

The critical velocity ratio M* is described by Goldmann [4] as follows:

$$M^* = \left(\frac{M^2 \frac{(\gamma+1)}{2}}{1 + M^2 \frac{(\gamma-1)}{2}} \right)^{1/2} \tag{4}$$

Specifying lower and upper surface velocities determines the circular arc radii R_l^* and R_u^* from Eq 4. Given β_i and β_u the inlet and outlet flow angles, the amount of turning in the circular arc region is given by the following equation [4]:

$$\begin{aligned} \alpha_{l,i} &= \beta_i - (\nu_i - \nu_l) \\ \alpha_{l,o} &= \beta_o - (\nu_o - \nu_l) \\ \alpha_{u,i} &= \beta_o - (\nu_u - \nu_i) \\ \alpha_{u,o} &= \beta_o - (\nu_u - \nu_o) \end{aligned} \tag{5}$$

The circular arc radii are now fully defined, so we can proceed with the computation of lower and upper transition arcs. The design is made with respect to non-dimensional axes x* and y*, both made dimensionless by dividing by r*. Both upper and lower surfaces are composed of two transition arcs (inlet and outlet) and a circular arc. For symmetric blades, the transition arcs are identical, thus the computation will be done only once. Even for asymmetric blades, the smaller transition arc amounts to a portion of the bigger transition arc, therefore only the big one needs to be computed. If ν_i is greater than ν_o, the inlet transition arc is the larger one.

The inlet transition arc is generated by computing small straight segments that deflect the flow angle and produce a certain variation of the Mach number. The computation starts at the end of the circular radii and proceeds towards the inlet. The coordinates are obtained from the intersection of the straight-line wall segments and the Mach lines for a given change in flow turning. The transition arc coordinates need to be rotated with an angle of $\alpha_{l,i}$ to have the final coordinates of interest. The velocity direction φ is related to the dimensionless radius R* as follows [4]:

$$\varphi = \pm \frac{1}{2} f(R^*) + Constant \tag{6}$$

Where:

$$f(R^*) = \sqrt{\frac{\gamma+1}{\gamma-1}} arcsin\left(\frac{\gamma-1}{R^{*2}} - \gamma \right) + arcsin\left[(\gamma+1) R^{*2} - \gamma \right] \tag{7}$$

Two different types of characteristics exist: the positive sign in Eq 6 gives the expansion lines whereas the negative sign gives the compression lines. Knowing that at x*=0, the velocity direction φ=0k, inlet and $R^*=R^*_{lower}$, the major vortex-expansion-characteristic equation is [4]:

$$\varphi = \frac{1}{2} [f(R^*) - f(R_l^*)] \tag{8}$$

If we make a discretization of the transition arc into k segments that deflect the flow with the same angle, the flow direction will be as follows [4]:

$$\varphi_{k,inlet} = \nu_{inlet} - \nu_{lower} - (k-1)\Delta\nu \tag{9}$$

The value of $f(R_k^*)$ can be written as a function of the dimensionless radius and $\Delta\nu$ [4],

$$f(R_k^*) = 2\nu_{inlet} - 2(k-1)\Delta\nu - \left(\frac{\pi}{2} \sqrt{\frac{\gamma+1}{\gamma-1}} - 1 \right) \tag{10}$$

For each k element, its coordinates along the major expansion characteristic can be determined using the following equations [4]

$$\begin{aligned} x_{k,inlet} &= -R^*_{k,inlet} \cdot sin\varphi_{k,inlet} \\ y_{k,inlet} &= R^*_{k,inlet} \cdot cos\varphi_{k,inlet} \end{aligned} \tag{11}$$

The equation of the transition arc segment (Eq 13) is determined by computing the slope of the segment, knowing each segment is a straight line parallel to the velocity direction [4]

$$m_{k,inlet} = tan\varphi_{k+1,inlet} \quad (12)$$

$$y^* = m_{k,inlet}\left[x^* - (x_l^*)_{k+1,inlet}\right] + (y_l^*)_{k+1,inlet} \quad (13)$$

The upper transition arc coordinates are computed in analogous manner to the lower transition arc coordinates and the equations are not reproduced further.

2. NUMERICAL VALIDATION OF VORTEX FLOW THEORY

Using the Supersonic Vortex Flow Theory described above, a MATLAB code was developed in order to generate the two-dimensional blade profiles and the shock wave distribution in the passage defined by the inlet transition arcs. Since the blade profiles are considered symmetric, the inlet and outlet Prandtl-Meyer angles are equal, thus only the inlet conditions as well as upper and lower Mach numbers must be specified as inputs. The program inputs were chosen as the same order of magnitude as the operating parameters of a pneumatic turbine starter suitable for gas turbines with maximum power output of 4MW (table 1)

Table 1. Input parameters for MATLAB code

β,[°]	M_i [-]	M_l [-]	M_u [-]	γ [-]
62.5	2.4	1.7	3.5	1.4

The non-dimensional blade profile and shock waves location calculated with MoC can be observed in Figure 1. The blade spacing G* and chord C* are obtained from the blade coordinates, in this case G*=0.554, C*=1.628.

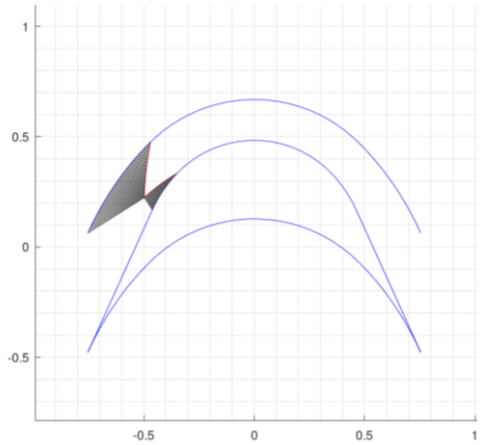

Fig. 1. Blade profiles generated in Matlab code

The theoretical profiles were validated in a two-dimensional CFD simulation in Ansys Fluent software. It was considered a fluid domain (Figure 2), in which the flow is stationary. The upper and lower edges of the domain were defined as periodic interfaces. After a thorough mesh dependency analysis, the final mesh geometry resulted with triangular 170 k elements, the smallest element has a size of 0.05mm. Even though quadrilateral elements help reduce considerably the computation time of the simulation, given the high turning of the flow and the sharp edges of the blades triangular elements are more suited in obtaining a good quality mesh. The mesh size has been refined until there has been no change in result parameters. The option for inflation near the wall provided by Ansys Fluent Meshing has not been an option because of the match control parameter needed for the periodicity boundary condition. Anyway, the meshing elements size has been reduced so much in order to achieve an y+ value smaller than 300 in almost all the regions of the computation domain. There are still small regions, where the velocity is really high, where y+ value has not been respected for k-ε turbulence model. In order to set the simulation in a 2D space, such as the MATLAB computation, the cell depth was set to zero in Fluent setup.

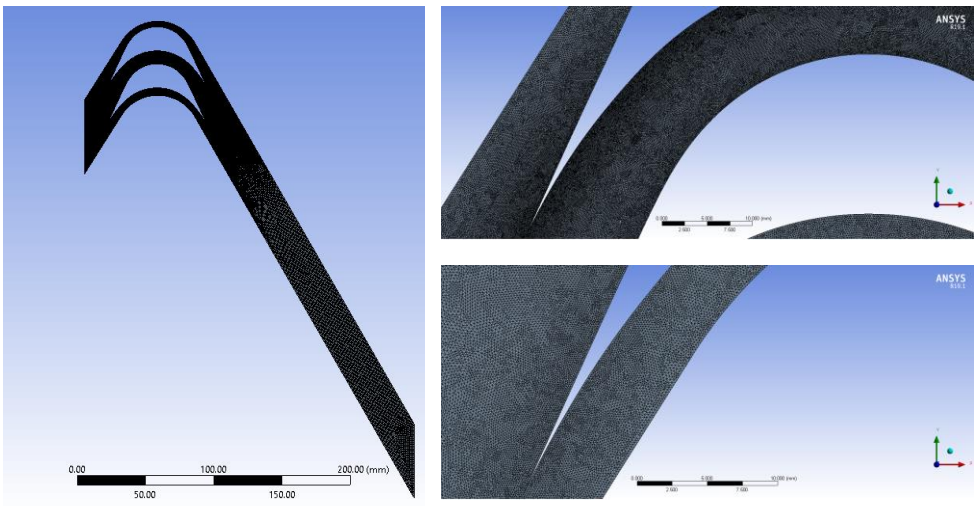

Fig. 2. Fluid domain mesh

For the computation, the k-epsilon turbulence model was considered, which is based on a RANS approach. The inlet boundary condition was defined as "velocity inlet" by components and the outlet was considered as "pressure far-field", as shown in table 2. The static pressure defined below is relative to the reference pressure.

Table 2. Boundary conditions for CFD simulation

	X Velocity [m/s]	Y Velocity [m/s]	Static pressure [Pa]	Mach number [-]	Temperature [K]
Inlet	366	784	501325	2.4	300
Outlet	-	-	0	0.01	300
Wall	No slip stationary wall				

The inlet velocity was calculated from the inlet Mach number (table 1), considering the air as ideal gas and the temperature 300 [K]. The reference pressure was set 101325 [Pa] and the viscous model used was "Realizable k-epsilon" in order to satisfy the high turbulence in the vortex flow region.

The converged solution for the Mach number and static pressure contours are shown in Figure 3 and 4. The static pressure profile obtained shows the development of the complex wave system at the inlet of the rotor. Comparing the location of the shock waves produced by the inlet transition arcs between the analytical calculation and the CFD simulation the maximum error is 4%. This error is within acceptable limits, and refers to the location of the intersection between the compression and expansion waves. The expansion waves are generated from the beginning of the upper transition arc, the error between CFD and MATLAB code being 0.7% in this case.

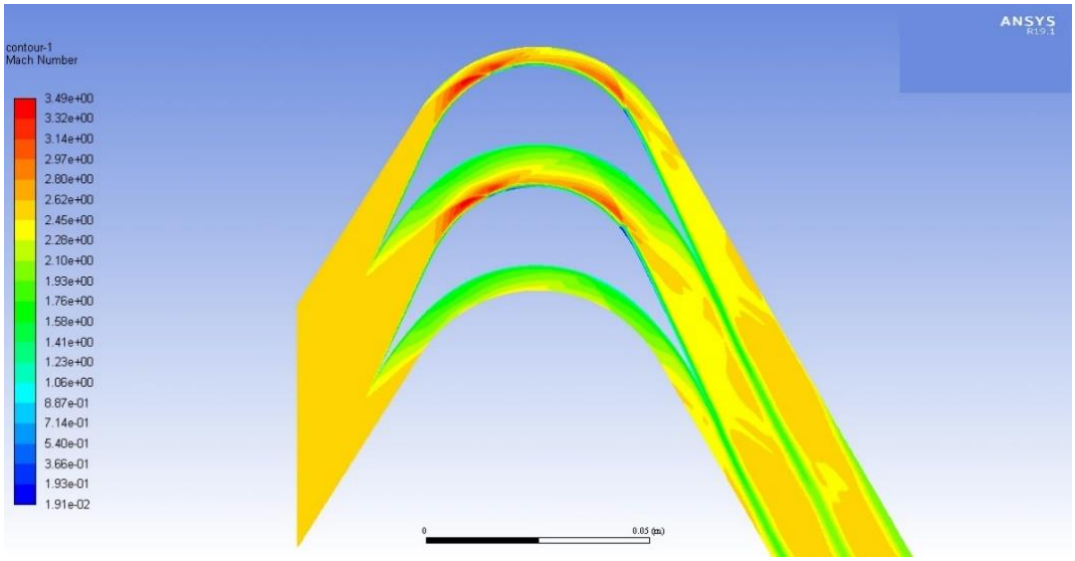

Fig. 3. Mach number contours

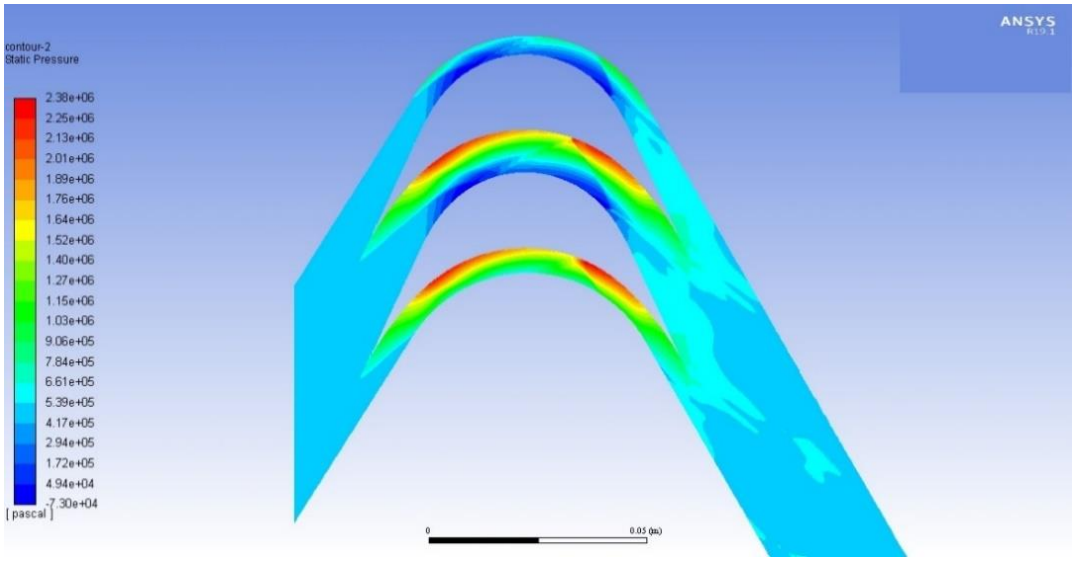

Fig. 4. Static pressure contours

The Mach number distribution along the fluid domain is in accordance with the analytical Mach distribution imposed during the computation phase. The fluid enters to rotor with 2.4 relative Mach number, it accelerates on the suction side of the blade passing through the expansion waves generated by the upper transition arc to a value of 3.5 relative Mach number, in the meantime on the pressure side of the blade the fluid passes through a series of compression waves that slow the fluid to 1.7 relative Mach number. The complex wave system generates the vortex flow behaviour of the fluid specific to the design method used. The difference between the upper Mach number and the lower Mach number is closely related to the loading on the blade, thus to the power produced by the turbine.

3. CONCLUSIONS

This article has presented the vortex flow theory, based on the method of characteristics, used to design supersonic rotor blades. The turbine rotor blades are composed of three main sections: inlet transition arcs that transform the uniform parallel flow into vortex flow inside the rotor; circular arcs that turn the vortex flow; outlet transition arcs that revert the vortex flow to uniform parallel flow. A MATLAB code has been developed to obtain the aerodynamic profile computed based on the given equations. The inputs of the code that determine the final geometry of the blade are of the same magnitude as the input parameters of a pneumatic turbine starter for gas turbines with maximum power output of 4MW. The differences between upper and lower Mach number are directly related to the loading of the blade, hence to the power output of the turbine. The static pressure input in the simulations is sufficient to obtain the imposed relative Mach numbers. Depending on the requirements of each application, the lower and upper surface Mach numbers can be manipulated to obtain the desired loading on the blade. CFD simulations have been performed in Ansys Fluent density-based solver. A mesh dependency analysis has been performed to establish the desired trade-off between computation time and mesh quality. The static pressure distribution shows the generation of the complex wave system at the inlet of the rotor, the differences between the location of the intersection between the compression and expansion waves amount to only 4%. The Mach number distribution in the fluid domain accurately reflects the imposed Mach number distribution in the analytical computations, meaning the lower and upper surface Mach numbers have been achieved by the flow passing through the complex wave system at the inlet. The boundary layer has not been taken into account in the analytical computations. Future research will have to compensate the boundary layer into the geometry of the blades in order to further reduce the error. This method of designing supersonic rotor blades can provide a better solution for changing existing pneumatic starters for gas turbines with new ones that are smaller and less heavy for the same power output.

REFERENCES

[1] Verneau, A. "Supersonic turbines for organic fluid Rankine cycles from 3 to 1300 kW." Von Karman Inst. For Fluid Dynamics, Small High Pressure Ratio Turbines 55 p(SEE N 88-14364 06-37) (1987).

[2] Seume, Joerg & Peters, M & Kunte, H. (2017). Design and test of a 10kW ORC supersonic turbine generator. Journal of Physics: Conference Series. 821. 012023. 10.1088/1742-6596/821/1/012023.
[3] G. Paniagua, M.C. Iorio, N. Vinha, J. Sousa, "Design and analysis of pioneering high supersonic axial turbines, International Journal of Mechanical Sciences, Volume 89, 2014, Pages 65-77, ISSN 0020-7403,
[4] Goldman LJ, Scullin VJ, 1968 "Analytical Investigation of Supersonic Turbomachinery Blading I - Computer Program for Blading Design", NASA Technical note TN D-4421. National Aeronautics and Space Administration, Lewis Research Center, Cleveland, Ohio.
[5] Noraiz M. et al "Design and Parametric Analysis of a Supersonic Turbine for Rotating Detonation Engine Applications"; International Journal of Turbomachinery Propulsion and Power 2022
[6] Chao FU et al. "Aerodynamic Design and Numerical Analysis of Supersonic Turbine for Turbo Pump" Internation Journal of Turbo&Jet Engines , Volume 33, Issue 3, September 2016
[7] Shin, B.-G. et al. (2005) "A Study on the Effect of Inlet Boundary Condition on Flow Characteristics of a Supersonic Turbine," International Journal of Aeronautical and Space Sciences. The Korean Society for Aeronautical & Space Sciences. doi: 10.5139/ijass.2005.6.1.001.

SUPERCIRCULATION STATOR, A PROOF OF CONCEPT

Valeriu DRAGAN[1]

Received: 07.03.2022
Accepted: 17.05.2022
Published: 06.07.2022

ABSTRACT: Conventional turbomachinery design has seen a plateauing of their technology readiness level in recent years, owing to the combined advances of CFD and AI methods. Hence, augmenting performances will require increasing integration of new techniques and secondary systems. This paper's goal is two-fold. On one hand it describes the initial attempt to integrate the concept of supercirculation into the vaned diffuser. On the other, it discusses the further extension of the concept and integration in other turbomachinery assemblies. To this effect, steady state 3D RANS calculations have been carried out on a generic cascade configuration with a blowing air injection slit on suction side of the airfoil's trailing edge. Previous 2D computations showed progress in eliminating the stagnation region near the trailing edge injector. Also streamline straightening was improved when compared to the baseline and circulation control configuration. Therefore, the paper has tested the 3D model of similar size and specifications, comparing only the supercirculation case against the baseline. It is the conclusion of this paper that supercirculation can indeed offer advantages over circulation control when applied in the context of cascades and that further work, both numerical and experimental are warranted to explore this concept.

KEYWORDS: Coanda Effect, Compressor Cascade, Active Flow Control, CEVA, CEPA

NOMENCLATURE

The notations and abbreviations will be defined in the text, as they appear.

1. INTRODUCTION

One of the priority problems acknowledged in the European Union, through the European Green Deal is that of greenhouse gases emissions. The short-term transition of automotive and road transport industry towards hybrid-electric propulsion requires downsizied internal combustion engines which rely on turbo/super-charging. Aviation propulsion represents a particularly difficult niche in the attempts to minimize climate impact because of the temperature, size and power density requirements of the existing power packs. As such, turbomachinery and in particular fans and compressors, will probably remain an important part of this industry. Therefore, an application of interest will be a medium size fan either as a stand-alone propulsion unit i.e. Electric Ducted Fan (EDF) or as a low pressure compressor stage for turboshaft/turboprop engines.

As CFD coupled with optimization techniques increase in accuracy and speed, they tend to be ubiquitous to turbomachinery design, reaching isentropic efficiencies in excess of 94% per rotor [1]. Hence, the current constructive types of components - or even the engine architecture itself - are likely to reach their full potential in the near future. As such, novel concepts might prove helpful in pushing the envelope further. One such technology is supercirculation (SC) [2], which uses the entrainment of thin curved wall jets subjected

[1] Romanian Research and Development Institute for Gas Turbines COMOTI

to the Coanda effect to increase airfoil loading. Supercirculation is supposed to hold potential beyond what is achievable by mere boundary layer flow control. Flow control methods have been used in both subsonic and supersonic [3] wing applications, with the effect of increasing its loading and stall angle, but also in experimental unconventional gas turbines [4].

The following research aims to bridge current know-how regarding SC in open flows with turbomachinery design methods. Since present understanding of highly curved wall jets is still incomplete, this research will attempt to shed light on the phenomenon outside its conventional use (open flows), possibly revealing hidden aspects that may have been, thus far, overlooked.

Envisioned advantages include:

-Increased blade loading - the ability to obtain the same pressure ratio with less or no back-sweep

-Reduction of the rotor diameter – hence a reduction in mass

-Reduction of the mechanical stresses (cheaper / lighter materials can be used).

-Reduction of the peripheral speed. hence less chances for shockwaves to appear on the vaned diffuser.

Stability-wise, a series of advantages emerge from the control over the flow angles. The blade inlet vortex shown in Fig. 1, which is developed at near stalling conditions is mitigated through the entrainment effect, improving the range and stability of the compressor.

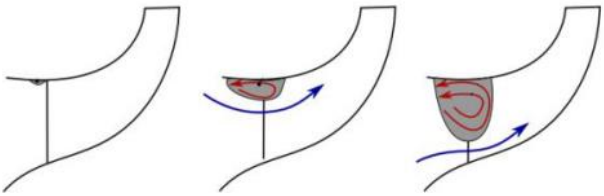

Fig. 1 - Off design-point recirculation bubble evolution near the tip of the blade inlet [5]

-The separation bubble occurring at the outlet is also mitigated by entrainment of the low velocity secondary flow. This is particularly important since a great percentage of the losses is caused by this secondary flow.

-Due to the reduced backsweep and also to the entrainment effects, the outflow of the compressor is less swirled, reducing the workload on the diffuser. Because of this, the diffuser blades can be made shorter and lighter, reducing their overall size and weight.

-Local shockwaves at the inlet due to streamline curvature effects are less likely to occur. Such a compressor will allow the engine designers to obtain higher pressure ratios and increase thermal efficiency without size and weight penalties. This will permit usage of parts such as intercoolers, heat recuperators or direct thermoelectric systems, which have not been used in aero-engines due to their size and weight.

2. LITERATURE SURVEY

Current fans and compressors, rely on rotating and stationary arrays of blades to deliver mechanical work to the fluid. One way to model this work exchange is Euler's equation for turbo-machinery which links the power delivered to the swirl velocity difference between the inlet and outlet of the particular array.

High pressure (HP) centrifugal rotors lead to higher swirled flows and often need multiple stator arrays [6] to deswirl the flow before the next stage or combustor. This limits the stability range of the machine since the flow angles only match the blade installation angles around the design point. To solve this, variable OGVs are used at the expense of size and weight Boundary layer control (BLC) methods have recently been used [7] on stators as proof that the range may be slightly increased by blowing thin wall jets from the trailing edge. Other authors, [8] have tried small blowing jets for BLC on highly cambered turbine vanes with similar results.

Building on previous unconventional concepts [9], the proposed supercirculation approach aims to use the more powerful entrainment effect - rather than simple BLC - to obtain even stronger flow turning/deswirling. Since the use of Coanda-effect has been linked to high entrainment rates, a classical way to achieve supercirculation is to use a thin wall jet over a curved surface near the trailing edge.

For radial compressor rotors near-leading edge blowing was tested in [10] proving some flow attachment capability. However this only tackles half of the stability and efficiency problem – the impeller inlet stall. Other methods such as passive flap like devices [11], co-flow actuation [12, 13] or even plasma actuation [14] have been researched for increased range. The Coanda effect has also been employed for other practical purposes such as active tip clearance control [15] or blade anti-icing [16], however the patents mention nothing about increasing stability or range. Figure 2 presents the theoretical differences between supercirculation and circulation control along with the streamline effect on a simple supercirculation airfoil.

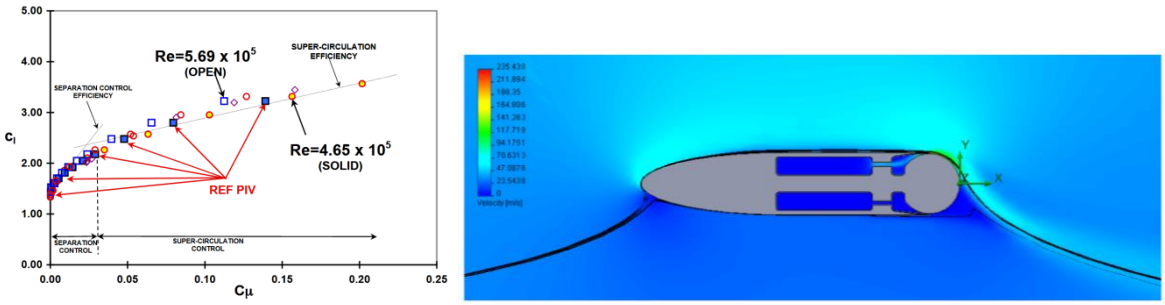

Fig. 2 – Lift coefficient for BLC and SC airfoil experimental data from Jones et al. [17] (left) and Supercirculation wing controls both leading and trailing edge flow angles [2] (right)

In Ref [7], a blowing pressure ratio is of around 1.2:1, as shown in Fig. 3, which is not a problem for the first stage - which is presented in the respective paper. However, this ratio might become problematic in higher pressure stages. Therefore, the reference value for the current study will be the pressure difference, rather than pressure ratio - which normally would have been a better metric for setting up the supercirculation boundary conditions.

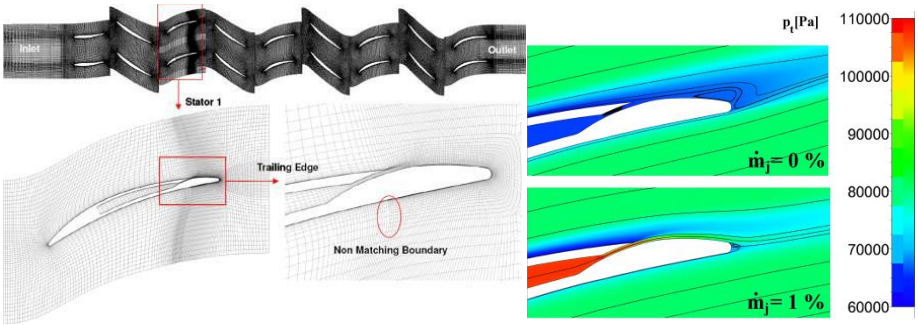

Fig. 3– Boundary layer control (BLC) stator vane used for axial compressors [7]

3. THE CFD STUDY

In order to test the effectiveness of the supercirculation (SC) method in bladed machinery, a linear cascade was considered and tested with CFD for its deswirling capability with and without SC. Since the cascade deswirls incomming flow and recovers some of the dynamic pressure, it can be assimilated with a compressor or fan vaned diffuser. Initially, a 2D batch was run with three turbulence models in order to assess their performance under the circumstances of the study. Afterwards, the 3D mesh was obtained by extruding the 2D mesh in the direction normal to the plane. Since this is a linear cascade, linear periodicity boundary conditions were placed on the sides of the domain. The 2D cases were run using Ansys Fluent because of the superior implementation of the RSM. However, after settling on the SST RC model for the 3D cases, the solver was switched to Ansys CFX which offers better convergence due to its turbomachinery specific features. The jet thickness and speed is identical in both BLC and SC methods so the energy consumption is identical.

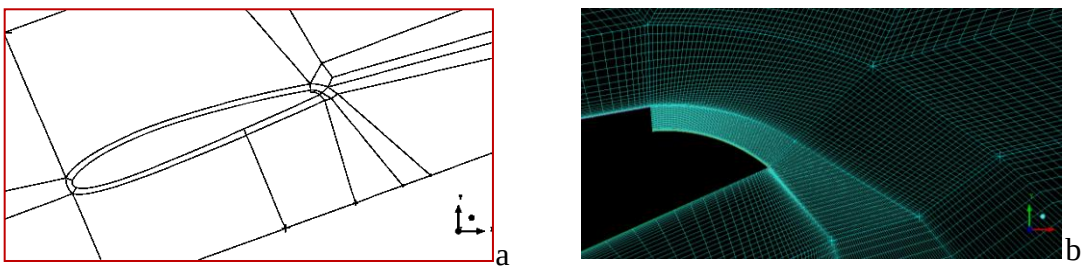

Fig. 4 The representative blocking structure (a) and the actual mesh (b) for the 2d cases

Figure 5 presents the pressure coefficient distribution on the airfoil and the Coanda ramp, relative to the total incoming flow pressure, for a more relevant comparison. On the pressure side of the vane, the RSM (Reynolds Stress Model) and SST RC (Shear Stress Model with Rotation and Curvature compensation) models

coincide well, whereas on the suction side the SARC (Spalart Allmaras with Rotation and Curvature compensation) and SST RC models appear to coincide. It would seem that for the strong positive streamline curvatures, in the first 40% of the chord, the RSM estimates a lower pressure drop, and for the moderate streamline curvatures, SARC behaves this way, relative to the SST.

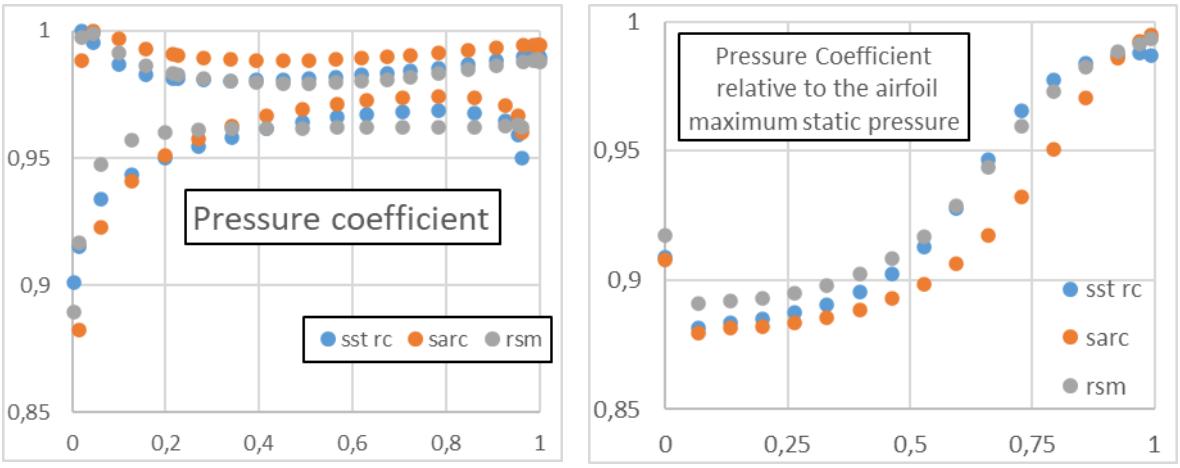

Fig. 5 Pressure coefficients for the airfoil (left) and Coanda ramp (right) from preliminary 2D RANS simulations with the three turbulence models tested (0-leading edge, 1-trailing edge)

The tipping point is located at around 40% of the airfoil chord, but this certainly will vary with different airfoils and cascade designs, so it should be regarded only as a reference. This observation holds for the Coanda ramp in Fig.5 (right) but because the curvature radius is constant, there is no tipping point where the three models switch. Since the SST RC was the only model which corresponded to any of the two, and due to its overall good track record of turbomachinery flow simulations, it will be the one chosen for the 3D simulations.

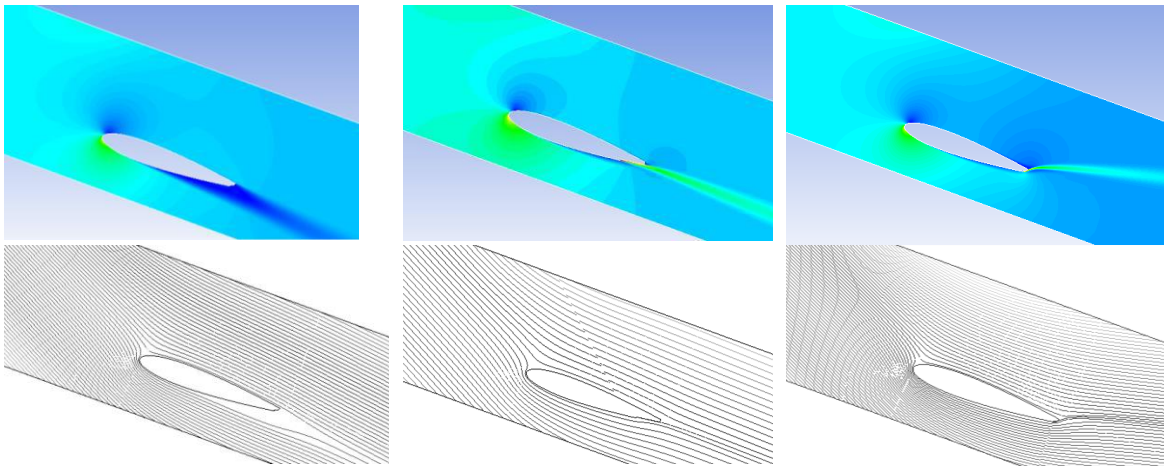

Fig. 6 Preliminary 2D study on conventional (left), BLC (center) and supercirculation outlet guide vane deswirling capacity from 40° incoming flow

In Fig.6, a comparison is made between the baseline, a boundary layer controlled (BLC) similar to Ref [7] and a supercirculation (SC) vane. It becomes apparent that for identical blowing conditions, although both flow control prevent the trailing edge stall observed in the baseline, the SC obtains substantially more deswirling than the BLC. This therefore justifies the choice for the 3D study focus on SC instead of BLC.

3.1. The 3D case setup

For the 3D CFD setup, the geometry was designed in keeping with the further work envisioned experimental setup. The blade is based on a NACA 2412 airfoil, with the rest of the relevant parameters presented in Table1 1. The ratio of the slit height to the ramp radius is kept at 15% and the ratio between the blowing velocity to incoming velocity is varied from 3:1 to 1:1 by increasing the incoming main stream velocity until it matches that of the blowing injector. The CFL=2 was chosen, in keeping with the recommendations from [18].

Table 1. Geometric and boundary parameters for the SC and baseline cases

Parameter	Value	Unit
Chord	**46**	**mm**
Blowin slit size (h)	**0.33**	**mm**
Coanda ramp radius	**2.21**	**mm**
Interblade space	**52**	**mm**
SC velocity to Inflow velocity ratios (u_j/u_∞)	**1:1; 2:1; 3:1**	

Turbulence was modeled using the Shear Stress Transport (SST) version of Menter's k-omega with rotation and curvature corrections, while air was modeled as an ideal fluid, with the temperature being influenced by viscous effects.

$$y = 6\left(\frac{u_{mx}\cdot\rho}{\mu}\right)^{-7/8}\left(\frac{x}{2}\right)^{1/3} y^{+} \tag{1}$$

$$Re_x = \frac{u_j\sqrt{1+\frac{2h\cdot f''(x)}{\{1+[f'(x)]^2\}^{3/2}}}\cdot\left(h+\pi\int_0^x\sqrt{1+[f'(x)]^2}\,dx\right)}{\mu} \tag{2}$$

Using Eq 1 , a first cell size order was computed in keeping with the prescriptions on the SST model, which ultimately depends on the local Reynolds number through the friction coefficient, wall shear stress and finally the shear velocity u_{mx}. A generalized local Reynolds number estimation via the CEVA/CEPA models is given by Eq.2 [19], depending on the function f(x) that describes the curve in question. Based on this, a safe value of 1 micron was set as a starting wall size for the entire contour of the airfoil. This was adopted in order to maintain overall inflation layer quality and not disrupt it at the SC injection site. A detail of the injection slit and adjacent Coanda ramp is presented in Fig.7, depicting the y+ distribution there and across the vane airfoil.

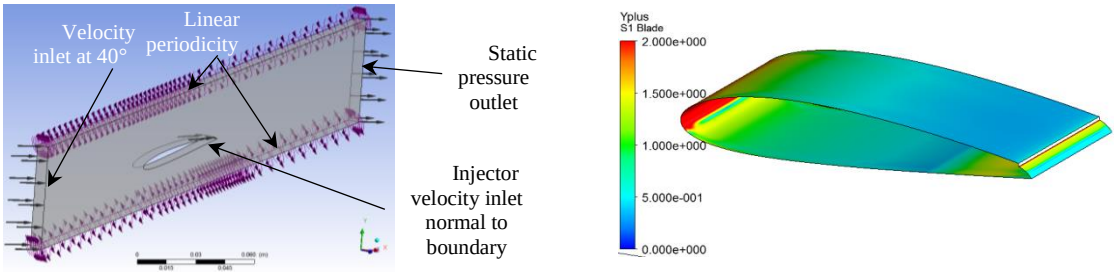

Fig. 7 - Boundary condition types (left) and wall y+ map on the airfoil and Coanda ramp (right)

Note that the pressure side near the trailing edge displays a higher than normal wall y+ value because of the blocking strategy. That is, in the trailing edge block, there is an increase in size of the near wall cell so that its height matches the length of the ramp cell. This helps convergence and prevents skewed and high aspect ratio cells. Results confirm increased deswirling of the incoming flow in the SC augmented cascade, along with good overall pressure losses, when compared to the baseline, as seen in Fig.8.

Figure 8 also depicts the velocity and pressure fields for the two extreme cases for the baseline and supercirculation. The top shows a 3:1 blowing velocity ratio while the bottom represents the 1:1 blowing ratio. As expected, as the blowing velocity and pressure decreases, the effects resemble more and more those obtained with the BLC technique. This is because the Coanda jet is more easily blown away from the ramp by the crossflow on the pressure side of the airfoil.

As marked, in Fig.8, the main use for the jet in this case would be in wake-filling, and to lesser extent for the slight entrainment of the suction side boundary layer. However, for the 3:1 velocity ratio we observe a significant influence on the main flow: near the leading edge the apparent incidence increases leading to a greater decrease in local static pressure on the suction side. Near the trailing edge, the suction side boundary layer is significantly energized due to the Coanda effect entrainment.

This extends the low static pressure zone towards the trailing edge on the suction side without flow separation. Near the trailing edge, the 3:1 SC jet is strong enough to act upon the main flow similarly to a fluidic flap. It is this action that leads to greater static pressure on the underside and consequently a clear increase in the apparent aerodynamic vane stagger angle. To a lesser extent, an increased incidence is observed.

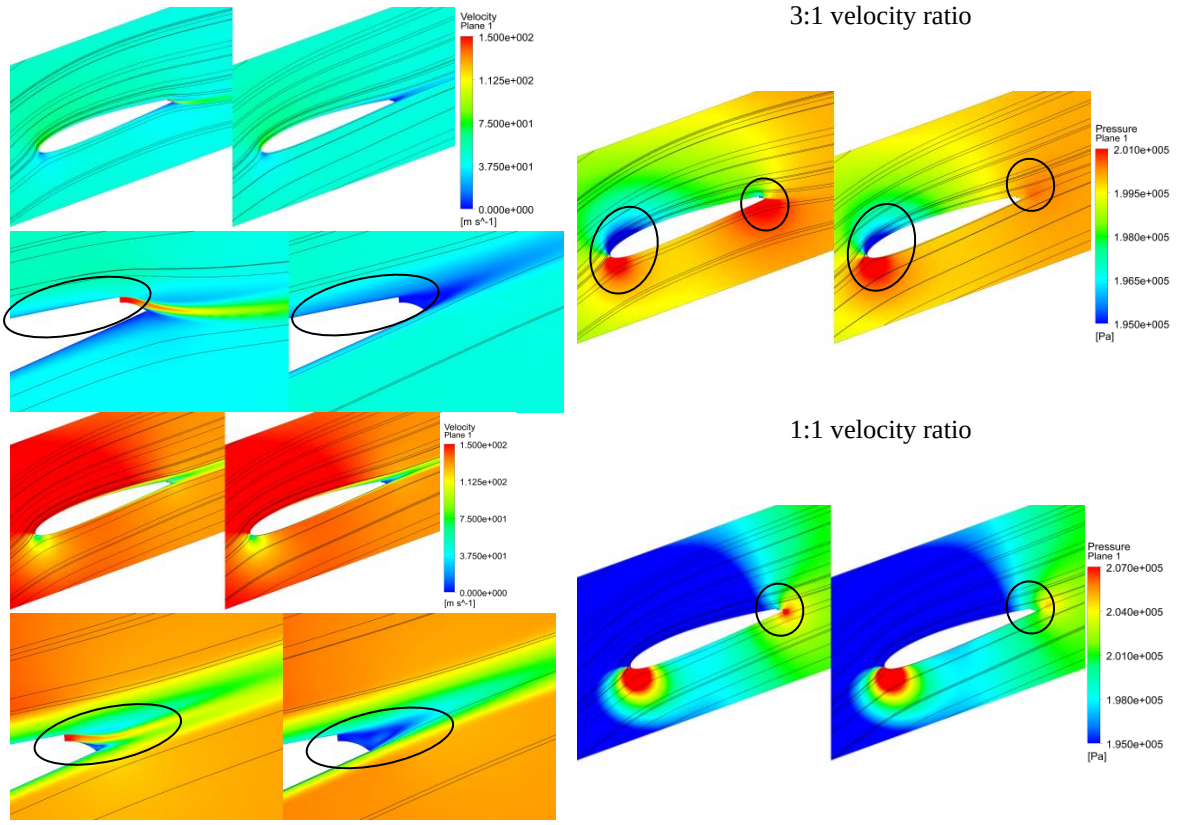

Fig. 8- Streamline distribution across the velocity and static pressure flow field of the Supercirculation augmented and the baseline cascade

4. CONCLUSIONS AND FURTHER WORK

Figure 9 presents the synthesis of global parameters for the 3D cases tested in this paper. The most interesting finding is perhaps the relative increase in mass flow compared to the baseline.

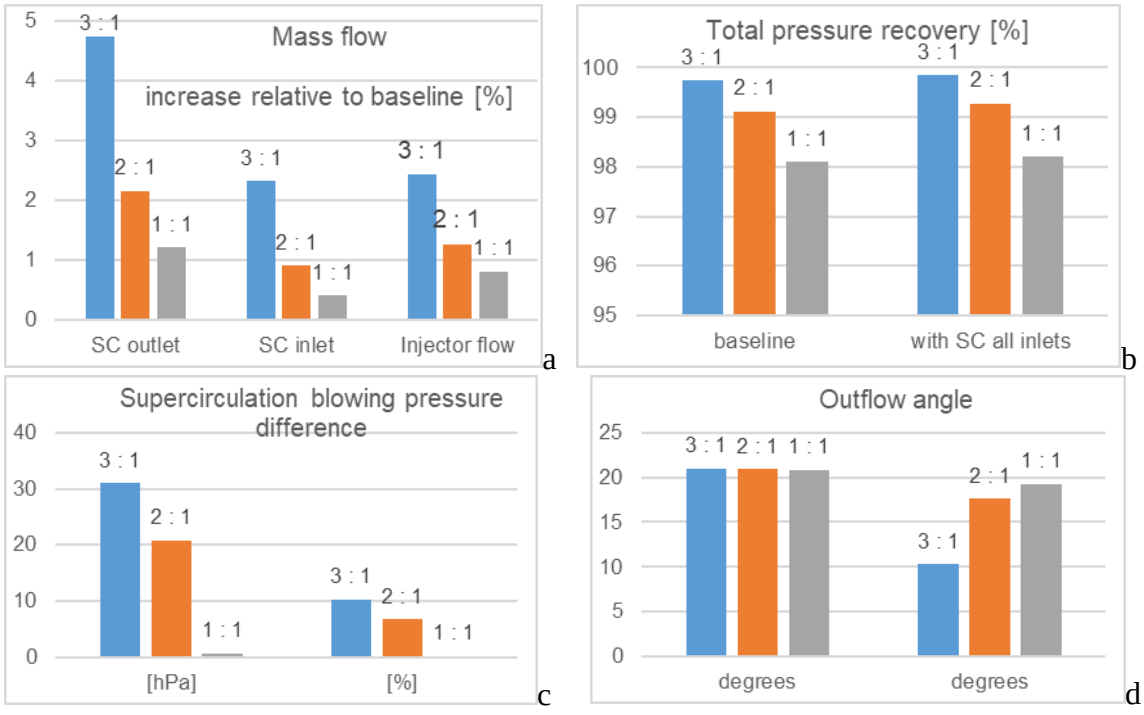

Fig. 9 - Baseline vs Supercirculation comparison for inlet to blowing speed ration for passage massflow (a), total pressure recovery (b), supercirculation blowing pressure (c) and outflow angle (d)

This is only in part due to the mass contribution of the SC jet, almost as much is obtained due to the rearranging of the flow around the vane. Since this is a passive organ, compressor efficiency cannot be calculated. Instead, the total pressure loss was looked at. Total pressure losses are slightly smaller in all supercirculation conditions, primarily due to the wake filling effect, independent of the velocity ratio and increased vane loading. In terms of pressure recovery, the supercirculation shows some insignificant improvement, well within the considered errors of the RANS technique. Deswirling is perhaps the most notable aspect of the SC improves upon, but is highly dependent on the velocity ratio.

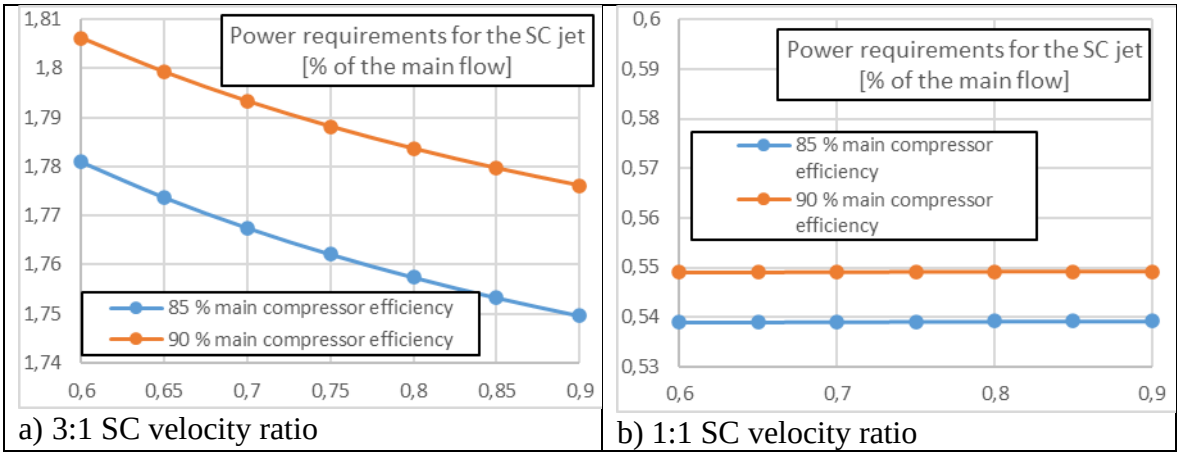

Fig. 10 - Power requirements for the SC jet for the 3:1 (a) and 1:1 (b), in percents relative to the estimated power of the main flow

In terms of energy expenditure, it needs to be pointed out that the energy put in through the supercirculation jet will be recovered - with some efficiency - in the outlet flow of the diffuser. Moreover, if the flow itself comes from a later compression stage - similar to the setup of Ref [7] there will be no need for any additional compression machinery. The same can be inferred if the flow comes from an organ where diffusion has occurred to a greater extent (e.g. a downstream plenum). Figure 10 shows the power requirements for the 3:1 SC jet, which obtained the maximum effect on the main flow as well as for 1:1 which obtained almost no significant effect. Since the stator is a passive organ, the main compressor efficiency had to be estimated to a realistic value between 85% - 90% . Also, since the bypass system for the SC flow is not yet defined geometrically, it's efficiency also had to be estimated to between 60%-85%. It can be seen that under these circumstances, the jet power requirements are between 1.75%-1.81% from the power requirements of the main flow. For the 1:1 velocity ratio case, the percentage was even lower, at around 0.55%.

4.1. Further work

A number of questions still remain unaddressed, such as what is the optimal blowing pressure ratio for a given incidence, the behavior at high Mach number or the influence of a greater span or spanwise incoming pressure gradients. The logical next step is a small scale experimental validation in a linear cascade similar to the one presented in Fig.11. All CFD tests presented here are especially designed with the height and overall dimensions of this future test rig in mind, considering the relative small available mass flow, pressures and temperatures. The test rig in this case will require a dedicated plenum and pressure source for the supercirculation blowing.

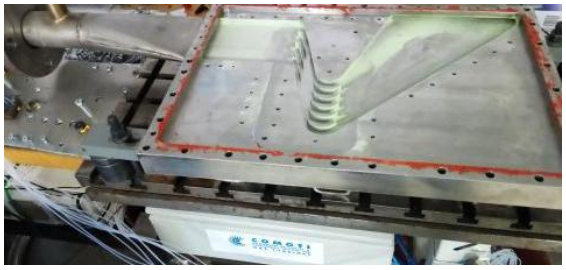

Fig.11 - CNC milled turbine test cascade [20]

Stationary guide vanes (IGVs and OGVs) as well as rotor blades can be designed with incorporated supercirculation slits. Stationary vanes might benefit from symmetrical trailing edge arrangements. Thus IGVs

can be made to provide different pre-swirls from hub to shroud to air entering the rotor. This could help reduce the blade setting angle differences between the hub and tip profiles of the rotor, giving it better stiffness and lower susceptibility to local accelerations due to the apparent streamline curvature effect. Figure 11 depicts such IGVs and OGVs.

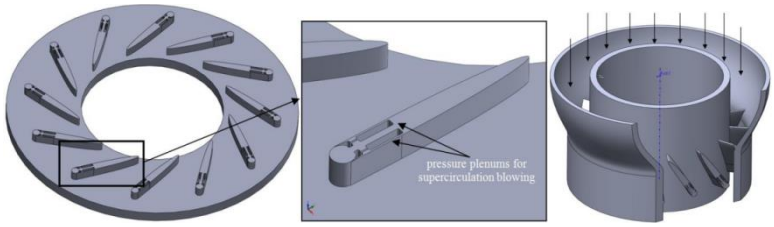

Fig. 12 - Supercirculation (SC) vaned diffuser (left) and Inlet Guide Vane (right)

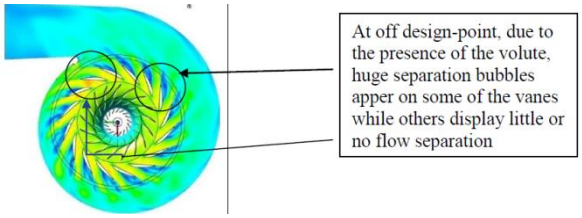

Fig. 13– The volute makes individual vanes work asymmetrically [21,22] leading to reduced performance

Such OGVs would be useful in automotive setups which use volutes. These are particularly problematic due to the inherent asymmetrical loading at off design point [12], as seen in the Fig.13. This cannot even be corrected with variable OGVs, but can be easily resolved by tailoring SC vanes to specific individual settings-giving the supercirculation augmented diffuser a qualitative advantage, allowing optimal control on the pressure distribution at the volute inlet, regardless of the operating point.

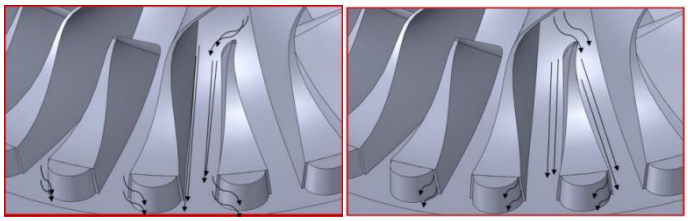

Fig.14 Super circulation augmented rotor blade used for stall delay (left) and chocking delay (right);

Self-supercirculation rotors have been proposed by [23] for enhancing helicopter lift. In compressors the physics will be different but the self-SC will mean no need for external compressors or cumbersome control systems. Figure 14 presents such an embodiment together with a proposed way to use it in extending the stable operation domain. Intuitively, for rotors an asymmetric trailing edge (TE) would seem the best choice for improving the stall margins. However a symmetrical TE would provide extended ranges at both stall and choking mass flows. Energy would be saved since much of the enthalpy of the recirculated air is not lost but put to work to compress the main flow.The supercirculation method – when applied to rotors – could address the impeller inlet stall but also the vaneless diffuser rotating stall.

REFERENCES

[1] V. Dragan, Aerodynamic reconfiguration and multicriterial optimization of centrifugal compressors – a case study, INCAS Bulletin, Vol. 6, Iss. 4 2014
[2] V. Dragan, Notes regarding the definition and applicability of supercirculation, INCAS Bulletin, Vol.6, Iss. 2, 2014
[3] R. Woszidlo, I.Wygnanski, Parameters Governing Separation Control with Sweeping Jet Actuators, 29th AIAA Applied Aerodynamics Conference, 2012

[4] GONG Hao, WANG Zhan-xue, LIU Zeng-wen, Study on thermodynamic cycle parameter matching for intercooled recuperated aero-engine, Journal of Aerospace Power 2012
[5] S. Mizuki and Y. Oosawa. Unsteady flow within centrifugal compressor channels under rotating stall and surge. Journal of Turbomachinery, 114 :312, 1992
[6] S A Korpela, Principles of turbomachinery, ISBN 9781119518082 1119518083 Hoboken, NJ, USA: John Wiley & Sons, Inc., 2020
[7] A.Vorreiter, S.Fischer, H. Saathoff, R. Radespiel, R. Seume, Numerical Investigations of the Efficiency of Circulation Control in a Compressor Stator, J. Turbomach 134(2), 021012 (Jun 27, 2011)
[8] Donald P. Rizzetta and Miguel R. Visbal, Numerical Study of Active Flow Control for a Transitional Highly Loaded Low-Pressure Turbine, J. Fluids Eng 128(5), 956-967 (Mar 09, 2006) doi:10.1115/1.2238877
[9] D. Japikse, K. Oliphant, D. Baun, Stability enhancement of compressors and turbopumps by passive flow control, Thermal &Fluid Analysis Works, College Park, MD, August 7-11, 2006
[10] A. Simpson, C. Aalburg, M.B. Schmitz, R.Pannekeet, V. Michelassi, F.Larisch, Application of Flow Control in a Novel Sector Test Rig J. Turbomach 136(4), 041002 (Sep 26, 2013) Paper No: TURBO-12-1249; doi: 10.1115/1.402490
[11] Yumeng Tang, Yangwei Liu, Lipeng Lu, Huawei Lu and Ming Wang, Passive Separation Control with Blade-End Slots in a Highly Loaded Compressor Cascade, AIAAJ Volume 58, Number 1January 2020
[12] Gecheng Zha, Yunchao Yang, Yan Ren, Brendan McBreen, Super-Lift and Thrusting Airfoil of Coflow Jet Actuated by Micro-Compressors, AIAA AVIATION Forum 2018 Flow Control Conference
[13] Riyadh I., AHMED,Harijono, DJOJODIHARDJO,Abd.Rahim, ABU-TALIB,Azmin, MOHD-RAFIE, Review on Progress and Application of Active Flow Control Devices - Coandă Effect on Unmanned Aerial Vehicles , PJSRR (2017) 3(1): 113-137
[14] Zhang Haideng, Wu Yun, Li Yinghong, Mechanism of compressor airfoil boundary layer flow control using nanosecond plasma actuation, nternational Journal of Heat and Fluid Flow Volume 80, December 2019, 108502
[15] Meheere D, Alecu D., Active tip clearance control system for gas turbine engine, Pratt and Whitney Canada, US 2019/0242303 A1, 2019
[16] Ivakitch R, Meheere D, Stone P, Fan blade anti-icing concept, Pratt and Whitney Canada, US 2021/0277826 2021
[17] G. S. Jones, C.-S Yao, B. G. Allan, Experimental Investigation of a 2D Supercritical Circulation-Control Airfoil Using Particle Image Velocimetry, AIAA-2006-3009.
[18] Trancossi M., Subhash M. Preliminary CDF Assessment of an Innovative Propelled Wing with Enhanced Performances by Coanda Effect. In: Ram M., Davim J. (eds) Modeling and Simulation in Industrial Engineering. Management and Industrial Engineering. Springer, Cham. (2018)
[19] V. Dragan, Reynolds number calculation and applications for curved wall jets, INCAS Bulletin, Volume 6, Issue 3/ 2014, pp. 35 – 41
[20]Cosmin Petru SUCIU, Cleopatra Florentina CUCIUMITA, Răzvan Edmond NICOARĂ, Mădălin DOMBROVSCHI1, SUPERSONIC PLANAR TURBINE CASCADE TEST BENCH, TURBO, vol. VII (2020), no. 2
[21] I.Malael, H.Dumitrescu, A.Dumitrache, Methods for Improve the Performance of the Turbomachines Using the Flow Control, ICNAAM 2011
[22] V. Dragan, Mihai Mihaescu, Proceedings of ASME Turbo Expo 2018: Turbomachinery Technical Conference and Exposition, GT2018, June 11-15, 2018, Oslo, Norway, GT2018-76165
[23] V. Dragan, Contributions regarding the design of a self super circulated rotary wing, ModTech 2012

SINCE 2019
TOGETHER AT
BSDA 2022
BUCHAREST, ROMANIA
SC ROMAERO SA, MAY 18-20, 2022

ARIE
Asociația Română a Industriei Elicopterelor

2022 BSDA
Black Sea Defense & Aerospace
EXHIBITION & CONFERENCE
8th Edition

TOGETHER FOR THE FUTURE OF THE
ROMANIAN HELICOPTER INDUSTRY
www.arieromania.ro

AEROFINA

COMOTI
ROMANIAN RESEARCH & DEVELOPMENT INSTITUTE FOR GAS TURBINES

Aerostar

IAR BRASOV

AIRBUS

TURBOMECANICA

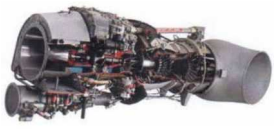

Black Sea
Defense, Aerospace and Security
International Exhibition

BUCHAREST, ROMANIA
ROMAERO S.A. - MAY 18 - 20 , 2022

COMOTI

The only specialized company that integrates such activities as

scientific research,
design,
manufacturing,
testing,
experimental activities,
technologic transfer and innovation

in the field of aircraft and industrial gas turbines and high speed bladed machinery.

220D Iuliu Maniu Ave., 061206 Bucharest, ROMANIA,
P.O. 76, P.O.B. 174
Phone: (+4)021/434.01.98, (+4)021/434.02.31, (+4)021/434.02.40
Fax: (+4)021/434.02.41, e-mail: contact@comoti.ro

www.comoti.ro